CHALMERS

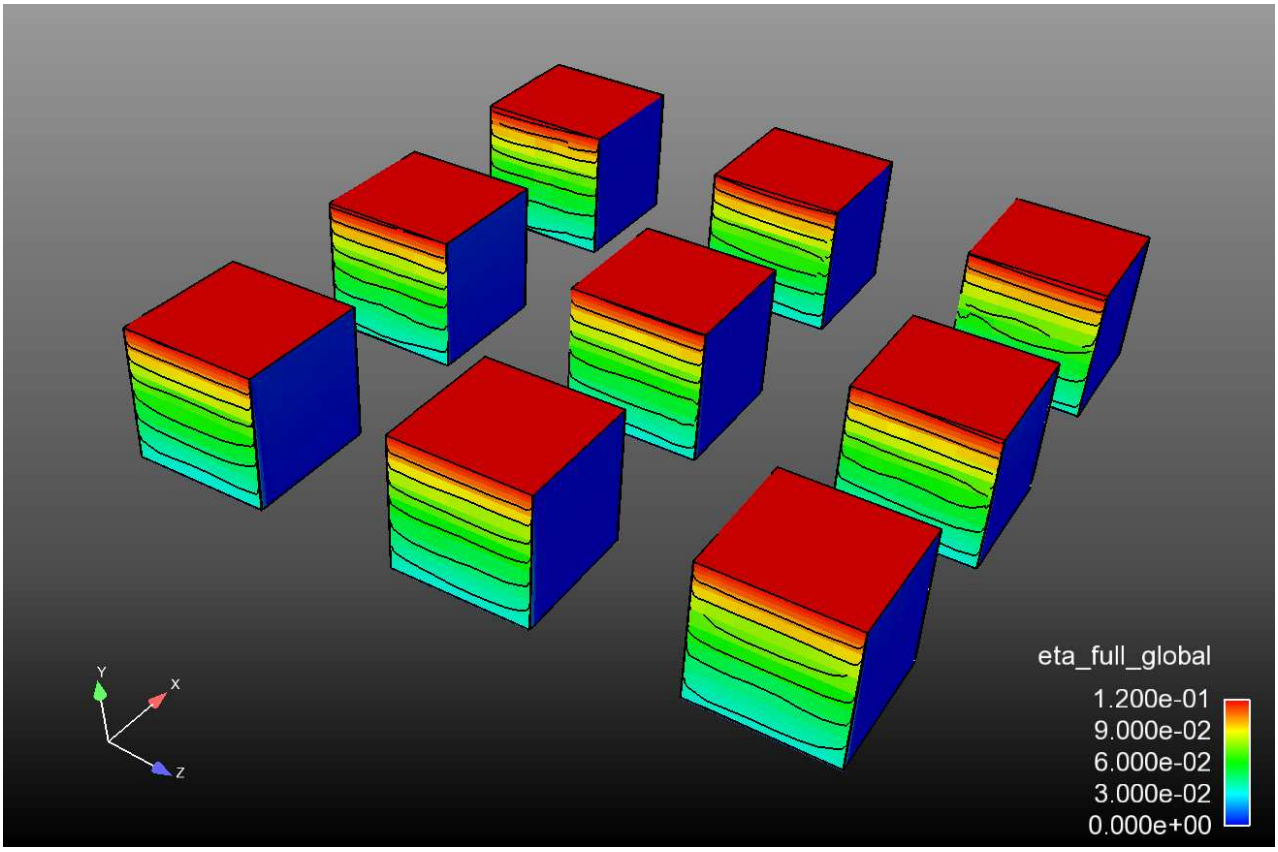

Simulating wind-driven rain on building facades using Eulerian multiphase with standard $k-\epsilon$ turbulence model

Master's thesis in Applied Mechanics

KAJ PETTERSSON

Department of Applied Mechanics
CHALMERS UNIVERSITY OF TECHNOLOGY
Göteborg, Sweden 2015

MASTER'S THESIS IN APPLIED MECHANICS

Simulating wind-driven rain on building facades using Eulerian multiphase with standard $k - \epsilon$ turbulence model

KAJ PETTERSSON

Department of Applied Mechanics
Division of Fluid Dynamics
CHALMERS UNIVERSITY OF TECHNOLOGY

Göteborg, Sweden 2015

Simulating wind-driven rain on building facades using Eulerian multiphase with standard $k-\epsilon$ turbulence model
KAJ PETTERSSON

Master's thesis 2015:87
ISSN 1652-8557
Department of Applied Mechanics
Division of Fluid Dynamics
Chalmers University of Technology
SE-412 96 Göteborg
Sweden
Telephone: +46 (0)31-772 1000

Cover:
Catch ratio η_{global} results for validation case using 4-phase model.

Chalmers Reproservice
Göteborg, Sweden 2015

Simulating wind-driven rain on building facades using Eulerian multiphase with standard $k-\epsilon$ turbulence model
Master's thesis in Applied Mechanics
KAJ PETTERSSON
Department of Applied Mechanics
Division of Fluid Dynamics
Chalmers University of Technology

Abstract

Wind-driven rain (WDR) is responsible for many types of damage to building facades and contributes to runoff management problems in urban environments. Consequently there is significant interest in predicting WDR using CFD simulations. In this thesis an Eulerian multiphase (EM) method is proposed which includes solving the rain phase closure equations instead of using a response coefficient to approximate turbulent behavior. The simulations are conducted using AVL FIRE with standard $k-\epsilon$ model and are validated against experimental data. The method produces results with error ranging from 1% to 50%, comparable to previous methods. In addition the use of no-slip boundary conditions on the facade walls causes artificially high levels of WDR, requiring numerical or methodological compensation.

Keywords: Wind-driven rain (WDR), Computational fluid dynamics (CFD) , Eulerian multiphase (EM), Standard $k-\epsilon$ model, Validation, Building facades, AVL FIRE

Preface

The research presented in this Master thesis paper was carried out at Chalmers University of Technology in Göteborg, Sweden. It is focused on the extension of previous work on using the Eulerian multiphase method to model wind-driven rainfall on building facades. The method is validated against experimental data and an application to a full-size building in Göteborg is presented. The work was carried out between April 2015 and October 2015 under the supervision of Sinisa Krajnovic at Chalmers Division of Fluid Dynamics and Angela Sasic Kalagasidis and Pär Johansson at the Chalmers Department of Civil and Environmental Engineering.

Acknowledgements

I would first like to thank my examiner Sinisa Krajnovic in Chalmers Division of Fluid Dynamics for his advice and assistance throughout the project as well as the input and enthusiasm of my supervisors Angela Sasic Kalagasidis and Pär Johansson from the Chalmers Department of Civil and Environmental Engineering, Division of Building Technology.

The completion of the project would not have been possible without the help of Guglielmo Minelli in Chalmers Division of Fluid Dynamics.

I would like to give a special thanks for the support from Zoran Pavlovic, Dr. Branislav Basara and Dr. Wilfried Edelbauer in Advanced Simulation Technologies at AVL.

Finally I would also like to thank my friends and family for their support, in particular Victor for his unwavering belief in my abilities.

Contents

1 Introduction

In recent decades there has been significant interest in predicting damage to building facades caused by factors such as facade soiling and erosion due to runoff, salt damage, frost, and vegetation growth [5]. These phenomena can effect the integrity of a building facade and also lead to cosmetic damage both on the exterior and interior of the building. One of the largest causes of these issues is moisture buildup on the facade during rain events. The rainfall exhibiting a horizontal velocity component caused by wind is termed wind-driven rain (WDR) and is the primary topic of this thesis paper. While there exist relatively complex models created to accurately predict moisture absorption by the building facade, namely the heat-air-moisture (HAM) model, they do not include the exterior aspects such as damage WDR can cause upon the building exterior. Therefore in more recent years as computational power has increased there have been developments in modeling WDR and a brief overview of the methodology is presented.

The method on which current research is based was pioneered by Choi in 1994 [11]. It consisted of the following steps and has been the main framework for all subsequent modeling of WDR.

- Solve the steady-state wind profile upstream of the building under study for desired wind speeds and directions.
- Calculate the trajectories of different size-class raindrops impinging upon the building facade.
- Calculate the amount of rainfall impinging on different "zones" on the building facade for different rainfall intensities and inlet wind profiles.

Choi used Lagrangian Particle Tracking (LPT) to iteratively solve the paths of different raindrop sizes such that these drops hit the building facade on the corners of the building facade zone. These four trajectories would define a stream tube in which he could calculate the distribution of different raindrop sizes and thus calculate the amount hitting the chosen facade zone. The stream tube is pictured in Figure 1.1.

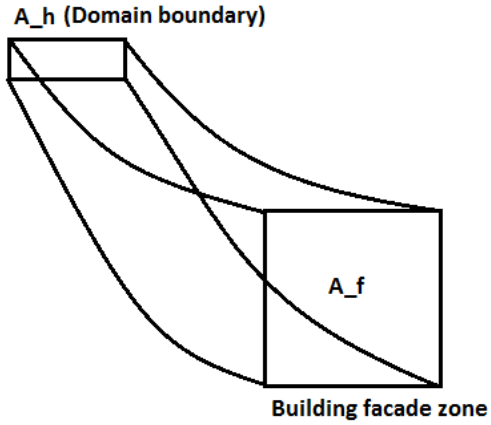

Figure 1.1: *Stream tube formed by raindrop trajectories.*

The amount of WDR on each facade zone was calculated using previous research on raindrop terminal velocities classified by raindrop size and raindrop size distribution dependent on rainfall intensity [12] [2]. The details of the method were formalized in 2002 by Blocken and Carmeliet [6] however they will be presented later in this paper as the method remains unchanged. Using LPT to solve the raindrop trajectories is extremely computationally intensive as each raindrop size trajectory must be solved for every zone, thus for complicated building geometries this method is very impractical. In addition the solution is unique for each rainfall intensity and each wind profile. These issues motivated subsequent researchers to modify the process in a variety of ways, both to increase accuracy and reduce computation requirements.

The first applications of Choi's technique that were validated against experimental data were published in 2002, 2006 and 2007 by Blocken and Carmeliet [6] [7] [8]. In the papers the researchers applied the method using steady-state 3D RANS with standard and realizable $k-\epsilon$ turbulence models, respectively. The results of their approach were compared with experimental data gathered at the VLIET test building of the Laboratory

of Buildings Physics, Katholieke Universiteit Leuven in Flanders, Belgium, with the results showing relatively good ability to predict WDR on the building facade. Due to the nature of the solution technique turbulent dispersion of the raindrops was omitted and was presented as a possible source of error. Another major advance in the technique was the extension of the steady-state model to a quasi-steady model, present in [6]. This meant that the solution for a particular wind profile, rainfall intensity and raindrop size selection was solved in the same manner as Choi, however the solutions are only computed for specific combinations above and the results are linearly interpolated to find the solutions for all other desired combinations. The idea behind this is that each zone is assigned a "catch chart" where the catch ratio is a function of wind speed and rainfall intensity. Given meteorological data on sufficiently small intervals the researcher can simply find the appropriate catch ratio value for the reported conditions and sum over all intervals during the rain event for each zone. This approach allows for much more flexibility when calculating the total rainfall impinging on a building facade under changing conditions rather than a single solution, thus increasing the model accuracy.

Up to this point no guidelines for applying CFD techniques to buildings in urban environments had been advocated and in 2008 Tominaga et. al. published a set rough guidelines to aid researches in modeling the wind profiles in an urban setting, thus helping to standardize the boundary conditions and turbulence models applied [22]. During the same year Blocken and Carmeliet published a paper detailing temporal accuracy standards for applying the quasi-steady WDR technique [3]. This paper showed that weather data must be collected and properly weighed such that the data was given in 10 minute intervals. Data provided in time intervals larger than this were proven to generate very inaccurate results when applying the technique to model entire rain events, lasting hours.

In 2009 Blocken et. al. tested 4 different turbulence models using the LPT approach on modeling the wind blocking effects on WDR between two buildings [10]. One building was a tower and the other a low-rise building. The results showed the wind blocking effect of the buildings reduced WDR on both buildings by around 25% where the blocking was in effect. Additionally the $k-\epsilon$ model performed most poorly compared to the realizable $k-\epsilon$, RNG $k-\epsilon$ and RSM models, with the RSM model giving the most accurate results. The failure of the standard $k-\epsilon$ lay in the over-prediction of turbulent kinetic energy along the roofline, thus giving inaccurate WDR results for the rooftop.

Another study was undertaken in 2009 by Akubu et. al. to determine the accuracy of the LPT modeling technique on WDR with winds oblique to the building facade [1]. The model was validated against data gathered at a site in Trondheim and the results suggested the technique to be less accurate when applied to oblique WDR than to WDR driven by wind normal to the building facade.

In 2010 Huang and Li published a paper detailing the replacement of LPT with Eulerian Multiphase (EM) to model the rain phases [13]. This alteration of the method by Choi was a means of eliminating the iterative raindrop trajectory calculations. In this method the rain is divided into different phases, each with a different raindrop diameter, and each phase has a corresponding volumetric ratio in its momentum equation. The conservation of mass and momentum equations are solved for each phase however turbulent dispersion is neglected.

In 2013 Kubilay et. al. published a paper using the model proposed by Huang and Li [14]. In the paper the turbulent dispersion term is neglected and the results are validated against the data gathered at the Hunting Lodge St. Hubertus in the Netherlands. The accuracy of the new method was comparable to that attained using the LPT however the computational resources were reduced significantly.

In the same year Blocken et. al. developed a method by which runoff on the building facade from WDR could be estimated, however the research presented in this paper was based upon the LPT method and was unvalidated [4].

In 2014 Kubilay et. al. released two papers on the application of the EM quasi-steady method to an array of cubes in close proximity to each other and to the Hunting Lodge St. Hubertus [17] [16]. The difference in the method from the previous work was the inclusion of the turbulent dispersion term, which is much easier to implement in the EM model than in the LPT model. The closure of each rain phase is attained by introducing a response coefficient which determines to what degree the rain phase velocity fluctuations align with those of

the wind phase. The solution for the domain is attained by iteratively solving the rain phase equations until the desired residual values are reached and the catch ratio is calculated from this solution for the entire building facade. The results of the simulation on the cubes was validated against detailed meteorological data gathered from a site in Switzerland [15] and the Hunting Lodge results were compared to the previous results from the simulation without the implementation of turbulent dispersion and the accuracy was shown to improve slightly in the new model.

Additionally Foroushani et. al. applied the LPT method to determine the effect of overhangs on the amount of WDR over the building facade [19]. The findings of this paper indicated smaller raindrops were drastically reduced in proximity to the overhangs however larger drops were largely unaffected.

While the results from these quasi-steady simulations have produced largely accurate results the expansion of the presented techniques to full multiphase simulations and other turbulent models has not been attempted (to this authors knowledge). In this thesis paper we will present an extension of the EM quasi-steady method by solving the turbulent closure equations for the rain phases. In Chapter 2 we will develop the theoretical background for solving WDR using both LPT and EM methods. Chapter 3 will outline the numerical approach and results for a validation case and in Chapter 4 a case constructed for the Skånegatan 1-3 complex in Göteborg, Sweden. Finally in Chapter 5 we will provide final thoughts and future recommendations for further research and implementation of the model presented in this paper.

1.1 Objectives

The main objectives for this paper are threefold: (1) to validate the EM method using standard $k-\epsilon$ model for all phases on a test case with experimental data, (2) to apply this method on a real building located in Göteborg, Sweden, (3) to assess the applicability of AVL FIRE to solving multiphase external flows such as the WDR calculations in this paper.

2 Theoretical background

2.1 Governing equations

The relevant equations in this paper are the Reynolds Averaged Navier-Stokes (RANS) equations. We provide a short summary of the derivation beginning with the standard Navier-Stokes equations for incompressible flow

$$\nabla \cdot \mathbf{u} = 0, \tag{2.1}$$

$$\frac{\partial \mathbf{u}}{\partial t} + \mathbf{u} \cdot \nabla \mathbf{u} = \mathbf{f} - \frac{1}{\rho}\nabla p + \nu \nabla^2 \mathbf{u}. \tag{2.2}$$

The time averaging requires that the instantaneous flow $\mathbf{u}$ and pressure must be split into mean and fluctuations as

$$\mathbf{u} = u_i = \overline{u}_i + u_i', \tag{2.3}$$

$$p = \overline{p} + p'. \tag{2.4}$$

where $\overline{u}_i$ represents the mean part of the directional flow and u_i' represents the fluctuations of the directional flow. By substituting (2.3),(2.4) into (2.1) and (2.2) and time averaging we get

$$\frac{\partial \overline{u}_i}{\partial x_i} = 0, \tag{2.5}$$

$$\frac{\partial \overline{u}_i}{\partial t} + \frac{\partial \overline{u}_i \overline{u}_j}{\partial x_j} = \overline{f}_i - \frac{1}{\rho}\frac{\partial \overline{p}}{\partial x_i} + \nu \frac{\partial^2 \overline{u}_i}{\partial x_j \partial x_j} - \frac{\partial \overline{u_i' u_j'}}{\partial x_j}. \tag{2.6}$$

Note that when time averaging $\overline{\overline{u_i}} = \overline{u}_i$, $\overline{u_i'} = 0$, $\overline{\overline{u}_i u_j'} = 0$ and $\overline{u_i' u_j'} \neq 0$. We rearrange some terms and remove the time dependent term, since it is unnecessary when we consider the equation is averaged in time already. The resulting system can be written as

$$\frac{\partial \overline{u}_i}{\partial x_i} = 0, \tag{2.7}$$

$$\frac{\partial \overline{u}_i \overline{u}_j}{\partial x_j} = -\beta(\overline{\theta} - \theta_0) g_i - \frac{1}{\rho}\frac{\partial \overline{p}}{\partial x_i} + \frac{\partial}{\partial x_j}\left(\nu \frac{\partial \overline{u}_i}{\partial x_j} - \overline{u_i' u_j'}\right), \tag{2.8}$$

where the force term is converted to the incompressible buoyancy term. This term will be neglected henceforth as we will assume adiabatic conditions and therefore no energy equation will solved. The time averaged fluctuation tensor (Reynolds stress) is unsolved in the equation system, thus we must generate additional equations for their exact values. The interested reader may find this process described in detail in basic turbulence modeling literature thus we will simply provide the final result

$$\frac{\partial \overline{u_i' u_j'}}{\partial t} + \overline{u}_k \frac{\partial \overline{u_i' u_j'}}{\partial x_k} = -\overline{u_i' u_k'}\frac{\partial \overline{u}_j}{\partial x_k} - \overline{u_j' u_k'}\frac{\partial \overline{u}_i}{\partial x_k} + \overline{\frac{p'}{\rho}\left(\frac{\partial u_i'}{\partial x_j} + \frac{\partial u_j'}{\partial x_i}\right)} - \frac{\partial}{\partial x_k}\left[\overline{u_i' u_j' u_k'} + \overline{\frac{p' u_j'}{\rho}}\delta_{ik} + \overline{\frac{p' u_i'}{\rho}}\delta_{jk}\right] + \nu \frac{\partial^2 \overline{u_i' u_j'}}{\partial x_k \partial x_k} - 2\nu \overline{\frac{\partial u_i'}{\partial x_k}\frac{\partial u_j'}{\partial x_k}}. \tag{2.9}$$

From this we must close the system of equations using some from of model. There are several available options however we will use the standard $k - \epsilon$ model due to its stability.

2.2 Standard $k - \epsilon$ closure model

By taking the trace of (2.9) and dividing by 2 we get the exact equation for k which represents turbulent kinetic energy. Now we must make some assumptions to remove the unknown terms and replace them with modeled terms.

$$\frac{\partial k}{\partial t} + \overline{u}_j \frac{\partial k}{\partial x_j} = -\overline{u_i' u_j'}\frac{\partial \overline{u}_i}{\partial x_j} - \frac{\partial}{\partial x_j}\left[\overline{u_j'\left(\frac{p'}{\rho} + \frac{1}{2}u_i' u_j'\right)}\right] + \nu \frac{\partial^2 k}{\partial x_j \partial x_j} - \nu \overline{\frac{\partial u_i'}{\partial x_j}\frac{\partial u_i'}{\partial x_j}}. \tag{2.10}$$

We utilize the Boussinesq assumption to provide closure for the Reynolds stresses, which states

$$\overline{u_i' u_j'} = -\nu_t\left(\frac{\partial \overline{u}_i}{\partial x_j} + \frac{\partial \overline{u}_j}{\partial x_i}\right) + \frac{2}{3}\delta_{ij} k. \tag{2.11}$$

Once incorporated into the exact k equation we can reduce the first term on the right hand side (the production term) to

$$\nu_t \left(\frac{\partial \overline{u}_i}{\partial x_j} + \frac{\partial \overline{u}_j}{\partial x_i} \right) \frac{\partial \overline{u}_i}{\partial x_j} = P^k. \tag{2.12}$$

The pressure diffusion term is removed due to the fact that it is negligible in comparison to the turbulent diffusion term. The triple correlation term is substituted with

$$\frac{1}{2}\overline{u_i' u_j' u_j'} = -\frac{\nu_t}{\sigma_k} \frac{\partial k}{\partial x_j} \tag{2.13}$$

We can now write the modeled k equation as

$$\frac{\partial k}{\partial t} + \overline{u}_j \frac{\partial k}{\partial x_j} = P^k + \frac{\partial}{\partial x_j} \left[\left(\nu + \frac{\nu_t}{\sigma_k} \right) \frac{\partial k}{\partial x_j} \right] - \epsilon, \tag{2.14}$$

where

$$\epsilon = \overline{\frac{\partial u_i'}{\partial x_j} \frac{\partial u_i'}{\partial x_j}}. \tag{2.15}$$

This term represents dissipation of energy and is unknown, therefore we must generate an exact equation for it or model it. The easiest method to generate the modeled ϵ equation is to apply dimensional analysis to the k equation and introduce appropriate coefficients on the right hand side of the equation such that the equation has the correct dimensions. In this way we can use the same assumptions as used to derive the modeled k equation to get the modeled ϵ equation

$$\frac{\partial \epsilon}{\partial t} + \overline{u}_j \frac{\partial \epsilon}{\partial x_j} = \frac{\epsilon}{k} c_{\epsilon 1} P^k + \frac{\partial}{\partial x_j} \left[\left(\nu + \frac{\nu_t}{\sigma_\epsilon} \right) \frac{\partial \epsilon}{\partial x_j} \right] - c_{\epsilon 2} \frac{\epsilon^2}{k}. \tag{2.16}$$

Finally we must define the turbulent viscosity and give numerical values to the coefficients. These are defined accordingly for the standard $k - \epsilon$ model.

$$\begin{aligned} \nu_t &= c_\mu \frac{k^2}{\epsilon}, & (2.17)\\ c_\mu &= 0.09, & (2.18)\\ \sigma_k &= 1.0, & (2.19)\\ \sigma_\epsilon &= 1.3, & (2.20)\\ c_{\epsilon 1} &= 1.44, & (2.21)\\ c_{\epsilon 2} &= 1.92. & (2.22) \end{aligned}$$

In addition the standard Launder & Spalding [18] wall functions are applied when necessary. The boundary conditions used for the wind are taken from wind engineering models and consist of vertical profiles for velocity, turbulent kinetic energy, turbulent intensity and dissipation.

2.3 Rain phase equations

2.3.1 Rain trajectories with LPT method

The rain trajectories are solved by injecting drops of a single diameter into the fully developed wind flow profile and calculating the equations of motion in time. The drops are assumed to be traveling at terminal velocity and their paths are calculated in time steps whereby the trajectory is refined iteratively until an appropriately unchanging R (relative Reynolds number) is found and the solution is used for the next timestep. This process must be done to find each individual drop path of interest and for each raindrop diameter. The equations of

motion for the raindrops are

$$m\frac{d^2x}{dt^2} = 6\pi\mu r\left(U-\frac{dx}{dt}\right)\frac{C_DR}{24}, \tag{2.23}$$

$$m\frac{d^2z}{dt^2} = 6\pi\mu r\left(W-\frac{dz}{dt}\right)\frac{C_DR}{24}, \tag{2.24}$$

$$m\frac{d^2y}{dt^2} = 6\pi\mu r\left(V-\frac{dy}{dt}\right)\frac{C_DR}{24} - mg\left(1-\frac{\rho_a}{\rho_w}\right), \tag{2.25}$$

$$m = \frac{4}{3}\pi r^3\rho_w, \tag{2.26}$$

$$R = \frac{2\rho_a r}{\mu}\sqrt{\left[\left(U-\frac{dx}{dt}\right)^2+\left(V-\frac{dy}{dt}\right)^2+\left(W-\frac{dz}{dt}\right)^2\right]}, \tag{2.27}$$

where U,V and W are the wind velocity components, m is mass of the raindrop, C_D is the drag coefficient of the rain droplet, ρ_a and ρ_w are air and water density respectively and μ is air dynamic viscosity.

The trajectories of interest are those that end at the corners of a designated area zone on the building facade and once these are solved a stream tube is defined from the initial positions on the boundary of the domain to the corners of the building facade zone.

2.3.2 Rain phases using EM method

The second modification to the method proposed by Choi was the substitution of LPT with Eulerian Multiphase for calculation of the rainfall. Once the wind profile is solved under steady-state conditions, the rain is divided into several continuous phases, each defined by a different raindrop diameter. Each phase has a corresponding volume fraction in its mass and momentum equations, represented as

$$\frac{\partial(\rho_w\alpha_k)}{\partial t}+\frac{\partial(\rho_w\alpha_k\overline{u}_{k,j})}{\partial x_j} = 0, \tag{2.28}$$

$$\frac{\partial(\rho_w\alpha_k\overline{u}_{k,i})}{\partial t}+\frac{\partial(\rho_w\alpha_k\overline{u}_{k,i}\overline{u}_{k,j})}{\partial x_j}+\frac{\partial(\rho_w\alpha_k\overline{u'_{k,i}u'_{k,j}})}{\partial x_j} = \rho_w\alpha_k g+\rho_w\alpha_k\frac{3\mu_a}{(\rho_w d)^2}\frac{C_dR}{4}(\overline{u}_i-\overline{u}_{k,i}), \tag{2.29}$$

where α_k is the volume fraction of kth rain phase, $\overline{u}_{k,i}$ the ith velocity component of kth rain phase, $\overline{u}_i$ the wind velocity component, ρ_w raindrop density, C_d raindrop drag coefficient and R the relative Reynolds number. Note in this equation the turbulent dispersion (turbulent mass flux) is included as the third term on the left hand side. We define the volume fraction α_k as

$$\alpha_k = \frac{R_h f_h(R_h,d)}{V_t(d)}\left(\frac{1\times10^{-3}}{3600}\right), \tag{2.30}$$

where $V_t(d)$ [m/s] is the terminal velocity of each raindrop size, R_h [mm/hr] is the horizontal rainfall intensity and $f_h(R_h,d)$ is the raindrop distribution through a horizontal plane. The relative Reynolds number can be calculated by

$$R = \frac{\rho_a d}{\mu_a}||\mathbf{u}-\mathbf{u}_k||, \tag{2.31}$$

where ρ_a is the air density and μ_a is the air dynamic viscosity. The closure for the turbulent fluctuations is attained by solving the $k-\epsilon$ equations for each phase by applying the Boussinesq assumption in the same manner as for the wind phase.

In previous research the equation system closure is attained by introducing a response coefficient. This

response coefficient is used in conjunction with the Boussinesq and the relevant relations are provided here.

$$-\overline{u'_{k,i}u'_{k,j}} = \nu_{t,d}\left(\frac{\partial \overline{u}_{k,i}}{\partial x_j} + \frac{\partial \overline{u}_{k,j}}{\partial x_i}\right) - \frac{2}{3}\delta_{ij}k_d, \tag{2.32}$$

$$k_d = C_t^2 k_a, \tag{2.33}$$

$$\nu_{t,d} = C_t^2 \nu_{t,a}, \tag{2.34}$$

$$\frac{\nu_{t,d}}{\nu_{t,a}} = \frac{1}{1+\frac{t_p}{t_{fl}}}, \tag{2.35}$$

$$t_p = \frac{4\rho_w d^2}{3\mu_a C_d R}, \tag{2.36}$$

$$t_{fl} \approx 0.2\frac{k}{\epsilon}, \tag{2.37}$$

where k_d is the kinetic turbulent energy of the dispersed phase, $\nu_{t,d}$ is the turbulent viscosity, C_t is the response coefficient, k_a is the turbulent kinetic energy of the air, t_p is the particle relaxation time and t_{fl} is the Lagrangian fluid time scale. The response coefficient is a relation between the velocity fluctuations of the continuous phase and the dispersed phase(s) and is a scalar since the velocity fluctuations are assumed to be isotropic. The particle relaxation time is defined as the response of particle acceleration to the relative velocity between the particle and continuum. The Lagrangian fluid time scale is simply defined to be the characteristic large eddy lifetime. The solution for the domain is attained by iteratively solving the rain phase equations until the desired residual values are reached.

2.4 Calculating WDR

Once the wind and rain flow equations have been solved the amount of WDR on the building must be calculated. The process is somewhat different for the LPT and EM models and each will be treated here.

2.4.1 LPT method

In order to calculate the WDR for each zone of the building facade the distribution of each raindrop diameter present in the air must be calculated. The formula for this was developed by Best in 1950 [2] and is based upon empirical fitting to experimental data and previous research by Gunn & Kinzer in 1949 [12]. The formula for the distribution is

$$F = 1 - exp\left[-\left(\frac{d}{a}\right)^n\right], \tag{2.38}$$

$$a = B_1 I^p, \tag{2.39}$$

$$W = B_2 I^q, \tag{2.40}$$

where F is the fraction of liquid water in the air with drops of diameter less than d [mm], I [mm/hr] is the rainfall intensity, W [mm^3/m^3] is the amount of liquid water per unit volume of air and the other variables are constants with values

$$B_1 = 1.30, \tag{2.41}$$

$$B_2 = 67, \tag{2.42}$$

$$p = 0.232, \tag{2.43}$$

$$q = 0.846, \tag{2.44}$$

$$n = 2.25. \tag{2.45}$$

Using this equation we can calculate the probability distribution $f(d)$ or fraction of water in the air with drops of diameter d to $d+\delta d$. The function $f(d)$ gives the probability density of each drop size, however due to difference in terminal velocity of each drop size we must convert this from size distribution in the air to size distribution through a horizontal plane. This conversion is accomplished using the following formula

$$f_h(d) = \frac{f(d)V_t(d)}{\int_d f(d)V_t(d)\mathrm{d}d}, \tag{2.46}$$

where $f_h(d)$ is the raindrop distribution through a horizontal plane. Once the distribution has been calculated we can define two measures of WDR, the specific catch ratio $\eta_d(d)$ and the catch ratio η which are given by

$$\eta_d(d) = \frac{R_{dr}(d)}{R_h(d)} = \frac{A_h(d)}{A_f}, \tag{2.47}$$

$$\eta = \int_d f_h(d)\eta_d(d)\mathrm{d}d, \tag{2.48}$$

where R_{dr} is the driving rain intensity (velocity of the raindrop normal to the building facade), R_h is the horizontal rainfall intensity, A_h is the area defined by the stream tube on the boundary dependent upon raindrop diameter and A_f is the zone area defined by the endpoints of the streamtube on the building facade. This catch ratio is the measure of WDR on the building facade, thus once this is calculated we arrive at our final solution. Note that in Choi [11] slightly different terminology is used however the method of calculation is identical, and since his terminology is no longer used we present only the current terms here.

This method of calculation can be extended for temporal (quasi-steady) WDR calculations by solving the problem for a particular wind profile, rainfall intensity and raindrop size selection. Catch ratio charts are constructed for each zone as functions of wind speed and rainfall intensity. Given meteorological data on sufficiently small intervals the researcher can simply find the appropriate catch ratio value for the reported conditions by applying linear interpolation and sum over all of the time intervals during the rain event. This approach allows for much more flexibility when calculating the total rainfall impinging on a building facade under changing conditions rather than a single solution. The downside of this extension is that the assumption of linear variation does not hold under all types of rain events and care must be used when making this assumption. The functions for the specific catch ratio and catch ratio are redefined as

$$\eta_d(d,t) = \frac{R_{dr}(d,t)}{R_h(d,t)}, \tag{2.49}$$

$$\eta(t) = \frac{R_{dr}(t)}{R_h(t)}, \tag{2.50}$$

and each timestep can be discretized as

$$\eta_d(d,t_j) = \frac{\int_{t_j}^{t_j+\Delta t} R_{dr}(d,t)dt}{\int_{t_j}^{t_j+\Delta t} R_h(d,t)dt} = \frac{S_{dr}(d,t_j)}{S_h(d,t_j)}, \tag{2.51}$$

$$\eta(t_j) = \frac{\int_{t_j}^{t_j+\Delta t} R_{dr}(t)dt}{\int_{t_j}^{t_j+\Delta t} R_h(t)dt} = \frac{S_{dr}(t_j)}{S_h(t_j)}. \tag{2.52}$$

2.4.2 EM model

The main difference in calculating WDR using EM methods is the utilization of the volumetric ratio α_k in the catch ratio equations. We therefore redefine the specific catch ratio and catch ratio as

$$\eta_d(k) = \frac{R_{wdr}(k)}{R_h(k)} = \frac{\alpha_{k,loc}|V_n(k)|}{R_h f_h(k)}\left(\frac{3600}{1\times10^{-3}}\right), \tag{2.53}$$

$$\eta = \int_d f_h(R_h,d)\eta_d\mathrm{d}d, \tag{2.54}$$

where R_{wdr} is the WDR intensity, R_h the horizontal rainfall intensity, $f_h(R_h,d)$ the raindrop size distribution through a horizontal plane and $|V_n(k)|$ the rain phase velocity magnitude normal to the building facade. These can be extended to the temporal domain in exactly the same manner as the catch ratios used in the LPT model.

2.5 Boundary conditions for atmospheric flow

We first treat the wind inlet profile equations and give a small theoretical background for their application. In wind engineering there are two widely used equation models for approximating the atmospheric boundary

layer (ABL) wind flow profile. These equations are known as the log-law and the power law equations, given in equations (2.55) and (2.56) respectively.

$$U(y) = \frac{u^*_{ABL}}{\kappa} \ln\left(\frac{y+y_0}{y_0}\right) \text{ for } y \leq 50\text{m}, \tag{2.55}$$

$$U(y) = u_r \left(\frac{y}{y_r}\right)^{\alpha} \text{ for } y \geq 50\text{m}, \tag{2.56}$$

where u^*_{ABL} is the ABL friction velocity, κ is the von Karman constant and y_0 the aerodynamic roughness length, u_r is a reference velocity taken at reference height y_r. α is an exponent determined by atmospheric stability. From these equations a profile can be constructed to approximate any wind profile providing a few factors are known and some meteorological measurements have been made at various heights from the ground in areas of interest. The aerodynamic roughness length is a theoretical measure of the height above the ground at which the wind speed becomes zero and is characteristic or the terrain roughness. This parameter is heavily dependent on the terrain upwind of the area of interest and has been approximated for various types of conditions based upon exhaustive data fitting and measurements [23].

In addition to the wind velocity profile we must also take into account the turbulent quantities. In this regard there has been work on finding appropriate inlet profile equations for k and ϵ that are valid for $k-\epsilon$ turbulence model under various atmospheric conditions. The equations used for the validation case in this paper are

$$k(y) = (I_u U(y))^2, \tag{2.57}$$

$$\epsilon(y) = \frac{(u^*_{ABL})^3}{\kappa(y+y_0)}, \tag{2.58}$$

$$I_u = 0.3, \tag{2.59}$$

where I_u is the streamwise turbulence intensity. In this case because our domain does not extend very high vertically in terms of general ABL computation we can assume it is constant.

Due to the domain height in the main case of interest we cannot assume a constant turbulent intensity, thus we use these alternate equations

$$k(y) = \left(I_u(y) U(y)\right)^2, \tag{2.60}$$

$$\epsilon(y) = C_\mu^{1/2} k(y) \frac{u_r}{y_r} \alpha \left(\frac{y}{y_r}\right)^{(\alpha-1)}, \tag{2.61}$$

$$I_u(y) = 0.1 \left(\frac{y}{y_G}\right)^{(-\alpha-0.05)}, \tag{2.62}$$

$$y_G = \frac{u^*_{ABL}}{6f}, \tag{2.63}$$

$$f = 2\Omega \sin(\lambda), \tag{2.64}$$

where α is the power law exponent, y_G is the boundary layer depth, f is the Coriolis force, Ω is the angular velocity of Earth's rotation and λ is the latitude of interest. This set of equations is presented by [22]. There are many different methods for approximating inlet conditions for wind and its turbulent quantities, the interested reader may find more information in [24] [21] [25].

3 Model 1: validation case

In order to validate the method described in this paper we compare our results against experimental data of a rain event gathered by Kubilay et. al. [15]. The experiment consisted of an array of 9 cubes set in a 3×3 matrix. Each cube is $H = 2 \times 2 \times 2$ meters and they are spaced 2 meters apart. The geometry is shown in figure 3.1. These cubes were placed in a parking lot at the Swiss Federal Laboratories for Materials Science and

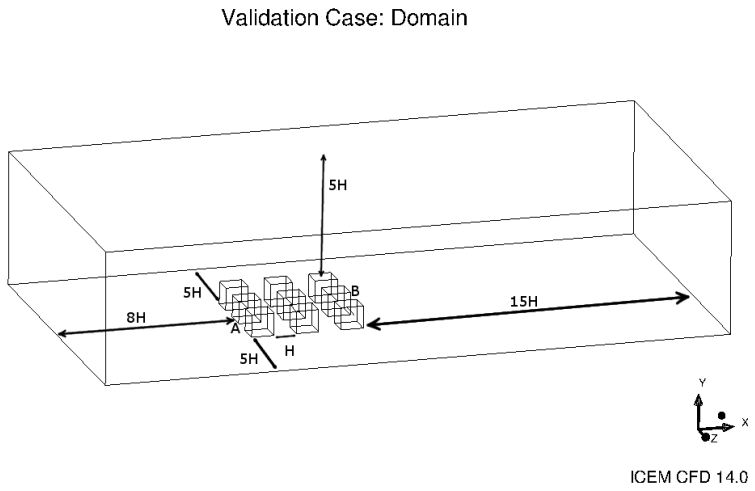

Figure 3.1: *Validation case computational domain.*

Technology (EMPA) in Dübendorf, Switzerland. The location has latitude 47°24′9″N and longitude 83°6′50″E. Special wind-driven rain gauges are affixed to 9 locations on the middle cube in the first row of cubes (Cube A) and 9 locations on the middle cube in the last row of cubes (Cube B). The cubes are positioned in such a way that the gauges face the prevailing wind direction (west). The wind speed and direction are measured by a 3D ultrasonic anemometer on a mast 8.4 meters high, located near the cubes and 2 cup anemometers at heights 2.4 and 5.4 meters high. 2 ultrasonic anemometers were also attached to the leading center cube for additional wind flow data. The horizontal rainfall is measured by a tipping bucket rain gauge that is located near the meteorological mast. The measurements are gathered for rainfall with frequency of 1 Hz and all data is averaged over 10 minute intervals for wind and rainfall.

In Table 3.1 we present the experimental data taken from the appropriate interval. Using this data we can

t [min]	U(y=2.4)	U(y=5.4)	U(y=8.4)	Wind dir.	R_h [mm/hr]	S_h [mm]
300	.541	.957	1.379	270.151	7.095	1.183

Table 3.1: Validation case experimental data.

construct the computational domain and appropriate boundary conditions for the simulation.

3.1 Domain

The computational domain measures 28H × 6H × 15H meters and the unstructured mesh consists of 1,013,249 hexahedral elements subject to the conditions in Table 3.2. The meshing is depicted in Figure 3.2 for the area of interest.

Dimension	Length [m]
$x(min)$	-16.0
$x(max)$	40.0
Δx	0.1184
$y(min)$	0.0
$y(max)$	12.0
Δy	0.0089
$z(min)$	-15.0
$z(max)$	15.0
Δz	0.0296
Δt	0.009

Table 3.2: Domain restrictions for validation case.

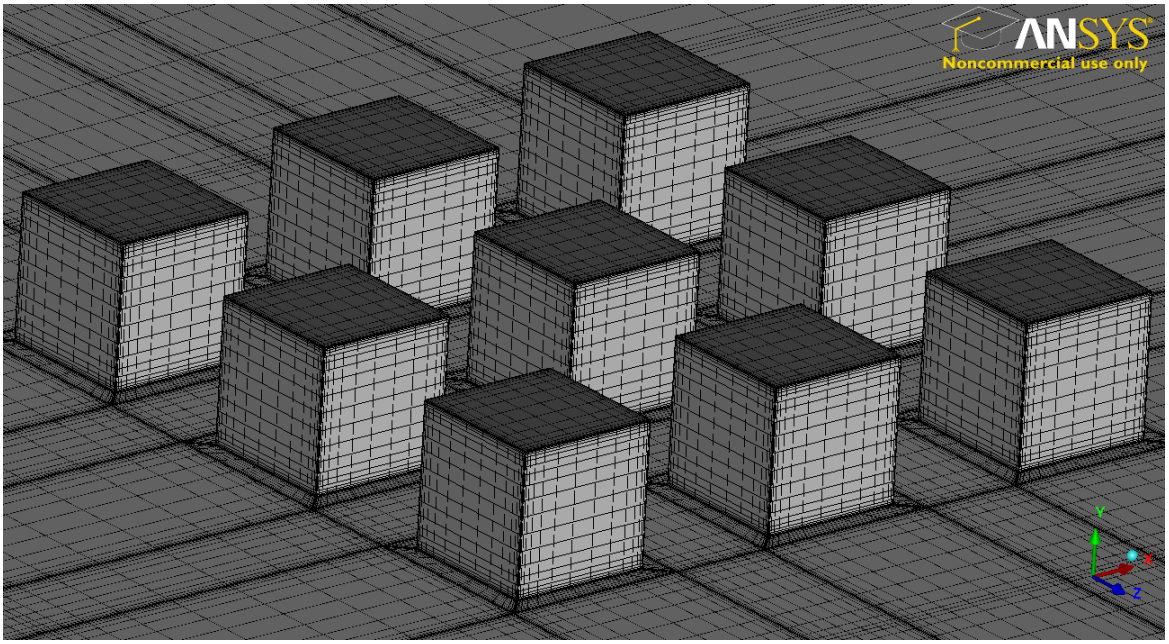

Figure 3.2: *Validation case mesh, cube array zoom.*

3.2 Wind phase B.C.s

The cubes are assigned no-slip wall boundaries with no roughness. The ground is treated the same as the cubes with the addition of a specified roughness height of 0.005 [m]. The roughness constant present in AVL FIRE is based upon the standardized sand-grain roughness scale created by Nikuradse in 1933 [20], this is left at 0.5. The inlet condition is treated using the atmospheric boundary layer (ABL) log-law formula below 50 meters, given in equations (2.57) - (2.59). The constants are assigned the following values for this particular case.

$$u^*_{ABL} = 0.1616, \tag{3.1}$$
$$\kappa = 0.42, \tag{3.2}$$
$$y_0 = 0.49. \tag{3.3}$$

We use a zero gradient condition on the outlet boundary. The top and sides of the domain are treated with symmetry conditions. It is noteworthy that there are alternative methods to specify the top boundary. Blocken et. al. recommend using defined flow parameters on the upper boundary to help preserve the flow profile [9]. When initializing the rain we alter this condition appropriately.

3.3 Rain phase B.C.s

The rain phase boundary condition for the cubes is identical to the wind case in our simulations. We include rain at the inlet condition with appropriate volumetric ratios, given in Table 3.3. The streamwise velocity of all rain phases matches the wind phase profile however each phase is assigned its corresponding vertical terminal velocity. The outlet and side conditions for the rain phases are the same as for the wind phase. We modify the wind phase boundary condition at the domain top from a symmetry condition to an inlet condition. The wind phase velocity and turbulent variables are assigned the calculated values for the top of the domain. The rain phases are assigned the same streamwise velocity and turbulent magnitudes as the wind phase however the vertical velocity is set as the appropriate raindrop size terminal velocity. In this manner we ensure the raindrops are traveling at their maximum speed while being correctly affected by the wind.

Phase #	α_k	d [mm]	V_t [m/s]
1 (wind)	.9999997142	-	-
2	7.50×10^{-8}	1.2	4.64
3	1.020×10^{-7}	2	6.49
4	1.088×10^{-7}	4	8.83

Table 3.3: Volumetric ratios of rain phases.

3.4 Simulation settings

The simulation is run in AVL FIRE in two stages. In stage 1 the wind profile is solved using steady-state semi-implicit method for pressure-linked equations (SIMPLE). We use the second order AVL Smart Relaxed discretization scheme for momentum, central differencing scheme for pressure (continuity) and first order upwind for turbulence. The wind phase is considered converged when pressure, momentum and the turbulent quantities reach scaled residuals of 10^{-6}.

In stage 2 we use an unsteady simulation with timestep $\Delta t = 0.005$ seconds and run until we reach acceptable convergence for the simulation. This implies monitoring mass flow, convergence of relevant variables and CFL number. We also monitor the phase velocities at specific locations to determine stability of the local flow. Note that SIMPLE/PISO solver is used instead of SIMPLE solver for increased stability. In addition to the momentum, continuity and turbulent equations we also solve a volume fraction equation using upwinding discretization scheme. Due to the very low volume fractions of rain in the air ($\alpha_k \leq 1 \times 10^{-7}$) the drag force of the drops on the wind is the only exchange from rain to wind phases [13].

3.5 Results

3.5.1 Wind phase solution

We present the steady-state solution for the wind profile in Figure 3.3. The profile is what we expect to see, with almost symmetrical flow around and between the cubes. Re-circulation occurs between the cubes, both in the streamwise and span-wise directions due to the separation of the flow. This phenomena serves to reduce WDR on the upper windward parts of the cubes behind others while increasing WDR on the lower back part of the cubes in front. It also disrupts the raindrop trajectories slightly, though due to our comparatively low wind speed the effect is not that significant in this model.

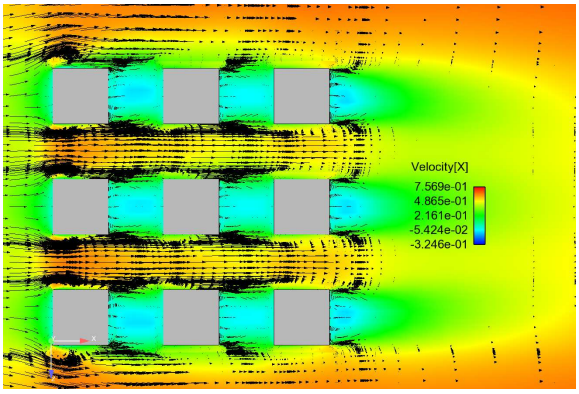

(a) *Streamwise wind velocity profile: y-cut.*

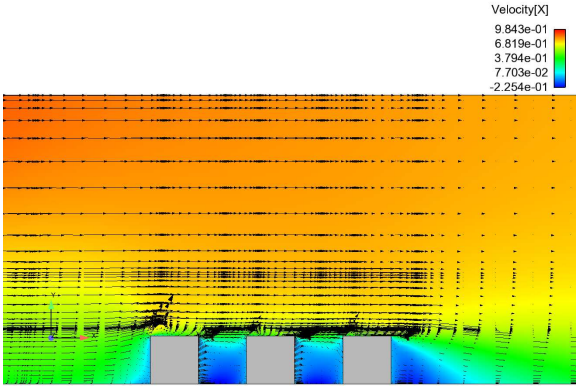

(b) *Streamwise wind velocity profile: z-cut.*

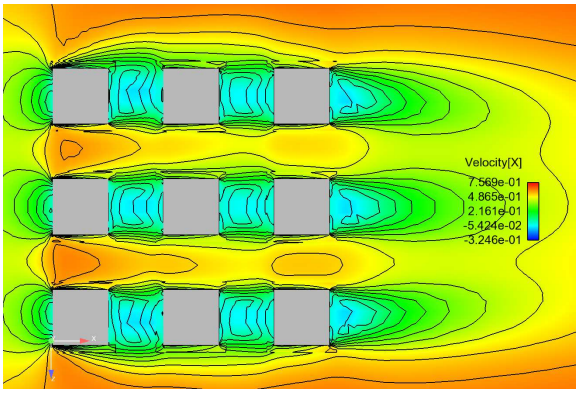

(c) *Streamwise wind velocity contour: y-cut.*

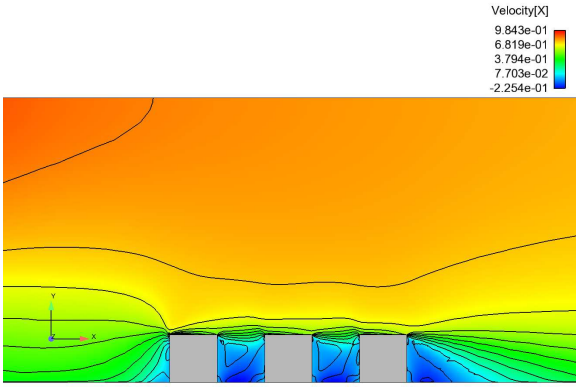

(d) *Streamwise wind velocity contour: z-cut.*

Figure 3.3: *Domain cuts showing wind velocity profile [m/s].*

3.5.2 Rain phase solution (4 phase)

In Figure 3.4 we show the trajectories of the rain phases used in the 4 phase mode. As we can see the trajectories for the smaller size raindrops are more heavily affected by the wind. Note that although the trajectories are affected they are not heavily disturbed. This is due to the generally low velocity of the wind in this case and the calculated distribution of drop sizes in the air. In this case the intervals are evenly distributed thus the smaller raindrop sizes are included in the smallest diameter represented here ($d = 1.2$ [mm]).

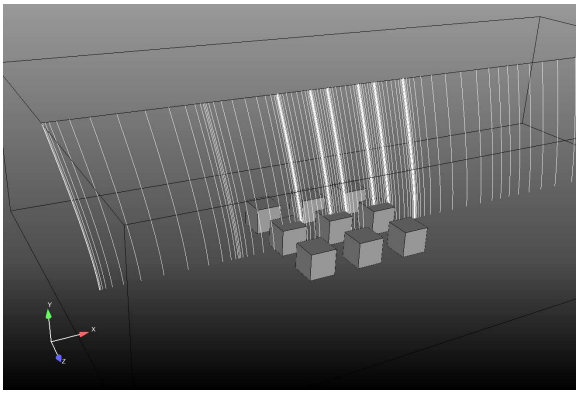

(a) *Rain trajectories,* $d = 1.2$ *[mm].*

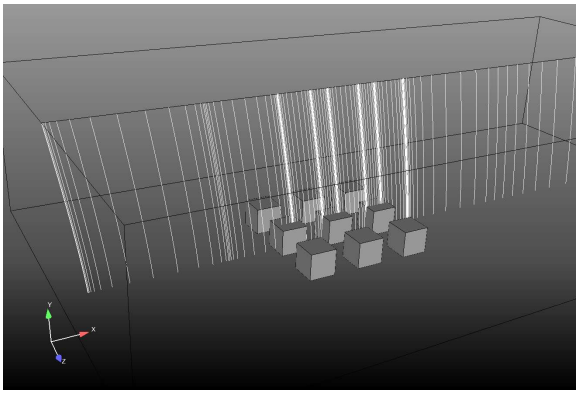

(b) *Rain trajectories,* $d = 2.0$ *[mm].*

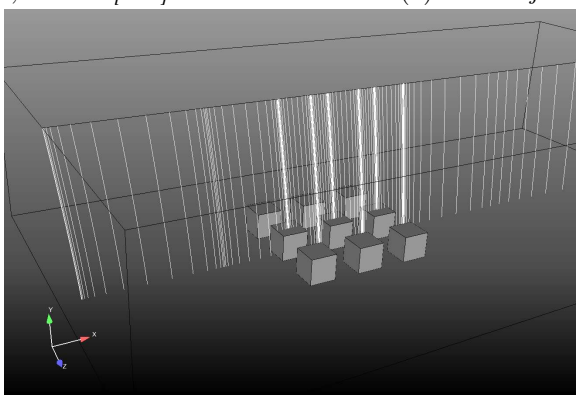

(c) *Rain trajectories,* $d = 4.0$ *[mm].*

Figure 3.4: *Rain phase trajectories along centerline of domain.*

The solution for the WDR on the cubes is calculated in two ways. In the first case the WDR is calculated using the global volumetric ratios found in Table 3.3. The second method uses the local volumetric ratio on the cube facade. The latter method is more realistic as the global ratio is a generalization and does not represent the changes occurring locally on the boundary. In Figure 3.5 the results for Cube A are shown using both methods and in Figure 3.6 we show the results for Cube B.

We see immediately the values of η using the local values are of a magnitude 100 times greater than those in the global case. This was investigated and the discrepancy is due to the boundary condition used on the cube walls in the simulation. The no-slip condition on these walls causes the rain to adhere to the wall faces during the course of the simulation and it is due to this that the values are significantly larger than those calculated using the global ratio values. In order to confirm this the local ratios were sampled 0.05 meters out from the cube face and the resulting values were indeed ≈ 100 times smaller than those directly on the cube face. To account for this difference the points for validation use the simulation volumetric ratios sampled 0.05 meters from the cube face in the correct position rather than those directly on the cube face and the results are shown in figures 3.5d and 3.6d.

In figures 3.5e and 3.5f we show the errors between the simulation results and experimental data gathered by [15]. The actual magnitudes of the error vary drastically, ranging from 9.7% to 56% on cube A and from 1% to 50% on cube B. This is within reasonable limits if we consider previous research in which the errors are not reported for a single time interval, only the cumulative results over an entire weather event are reported. In addition the quasi-steady method used in previous work involves substantial use of linear interpolation, which

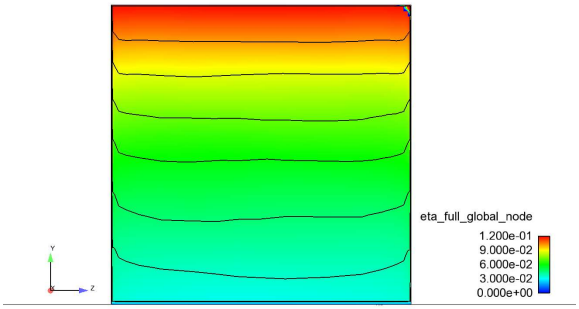

(a) η_{global} *values for cube A.*

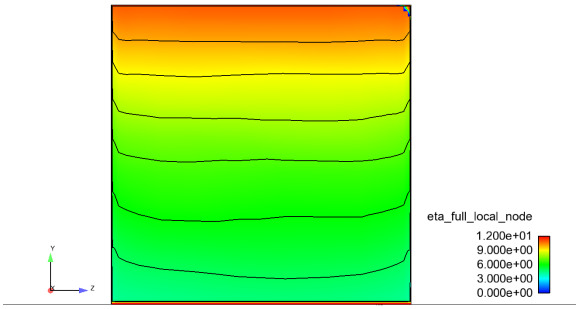

(b) η_{local} *values for cube A.*

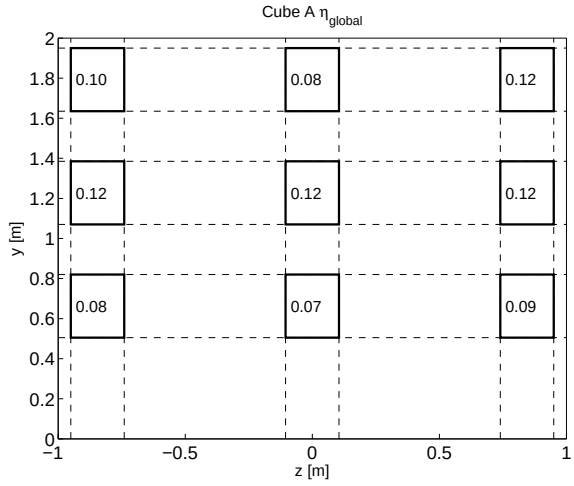

(c) *Simulation measurements at validation points on cube A.*

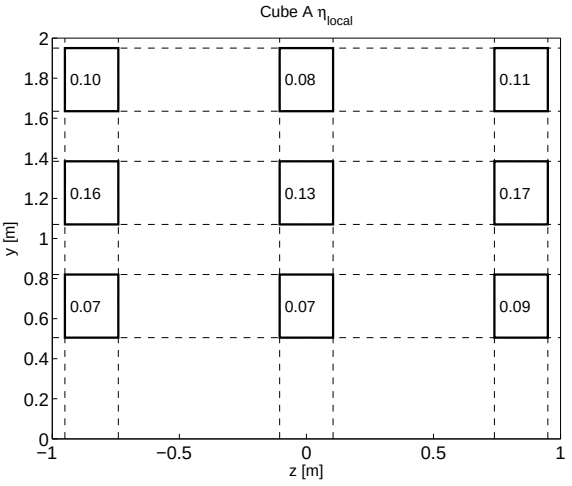

(d) *Simulation measurements at validation points on cube A.*

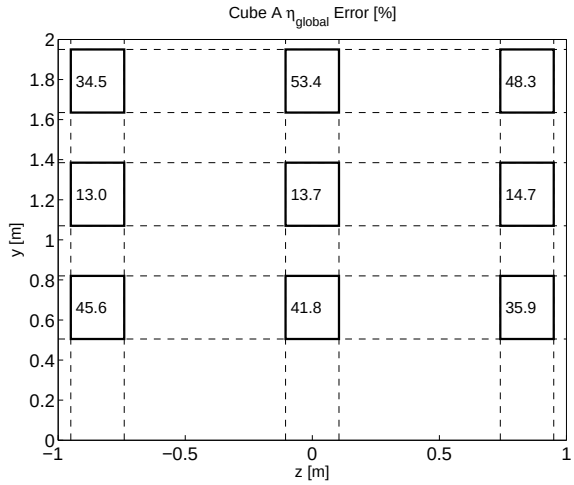

(e) *Error [%] between experiments and simulation:* η_{global}.

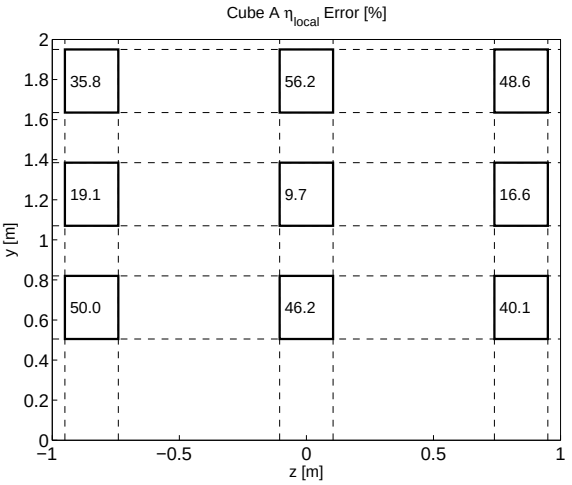

(f) *Error [%] between experiments and simulation:* η_{local}.

Figure 3.5: *Validation case results: Cube A, 4 phases.*

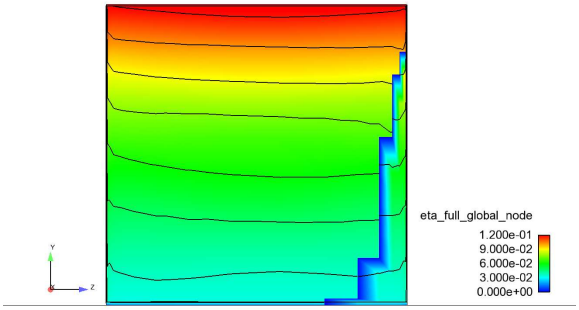

(a) η_{global} *values for cube B.*

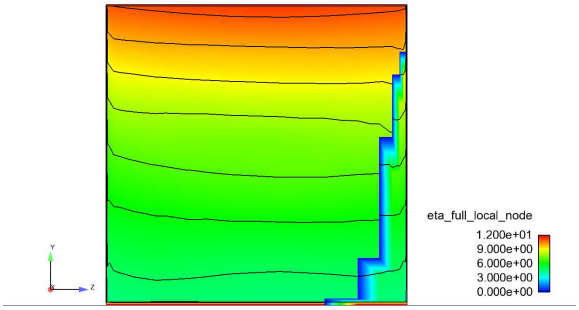

(b) η_{local} *values for cube B.*

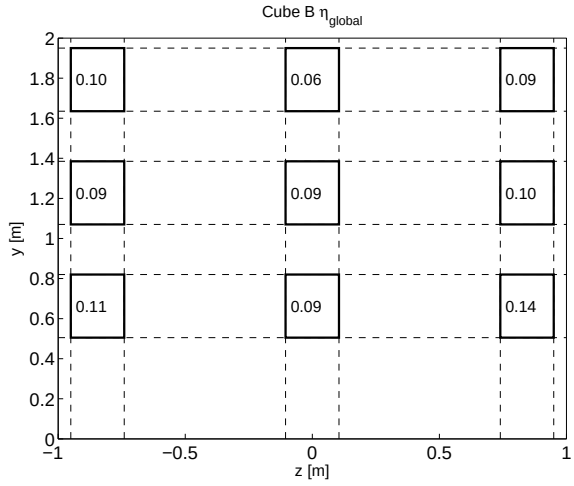

(c) *Simulation measurements at validation points on cube B.*

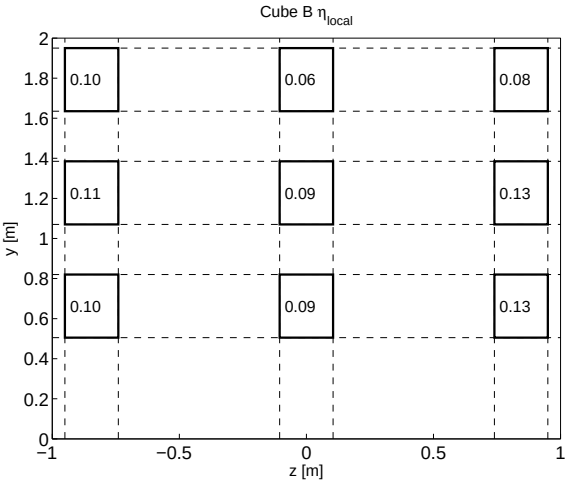

(d) *Simulation measurements at validation points on cube B.*

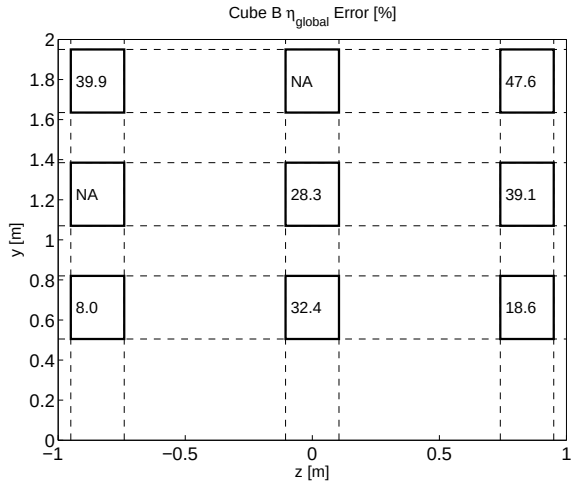

(e) *Error [%] between experiments and simulation:* η_{global}.

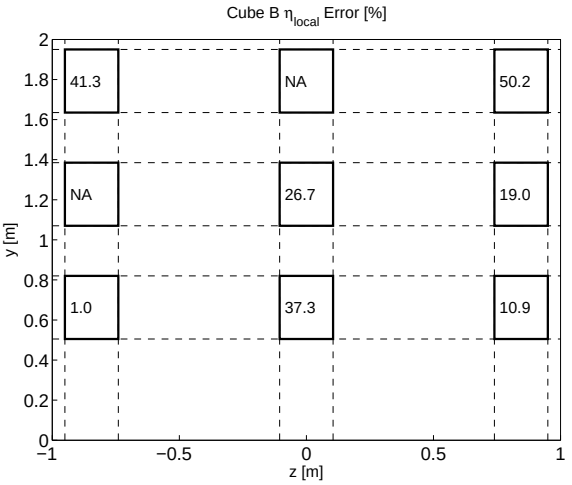

(f) *Error [%] between experiments and simulation:* η_{local}.

Figure 3.6: *Validation case results: Cube B, 4 phases.*

can cause errors that are hard to isolate. By taking the measured values for 1 time interval and comparing them against the results of the simulation we get a more accurate idea of the validity of our approach. There remain several sources of error in this model. The most obvious are number of rain phases (the idea is more variety in diameter should improve results) and the turbulence model being used. In this paper we only consider the case of more rain phases, presented in the next section.

3.5.3 Rain phase solution (8 phase)

We extend the previous solution by including 8 phases rather than 4. The simulation is set up identically to that of the 4 phase and the same steady-state wind solution is used. The new phase information is given in Table 3.4.

Phase #	α_k	d [mm]	V_t [m/s]
1 (wind)	.99999968758	-	-
2	1.296×10^{-8}	0.5	2.06
3	2.293×10^{-8}	0.8	3.27
4	4.605×10^{-8}	1.2	4.64
5	5.595×10^{-8}	1.6	5.65
6	5.554×10^{-8}	2.0	6.49
7	9.260×10^{-8}	3.0	8.06
8	2.634×10^{-8}	4.0	8.83

Table 3.4: Volumetric ratios of rain phases.

Since the wind profile is the same as in the 4 phase case we begin our analysis with the trajectories of the increased number of phases. A sampling of the trajectories are shown in Figure 4.5. We can see immediately

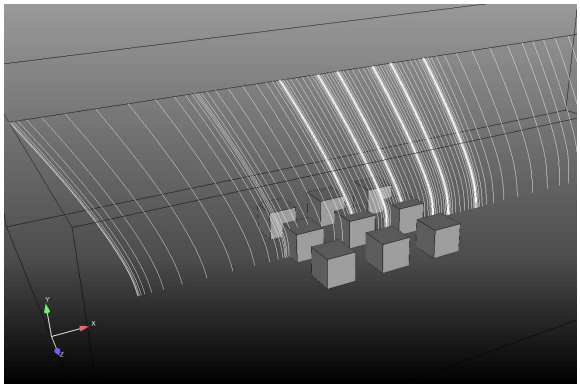

(a) *Rain trajectories, $d = 0.5$ [mm].*

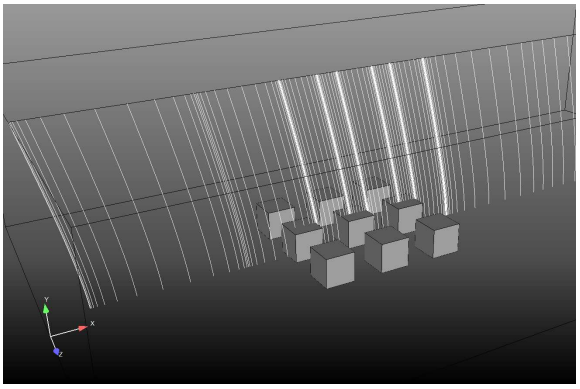

(b) *Rain trajectories, $d = 1.2$ [mm].*

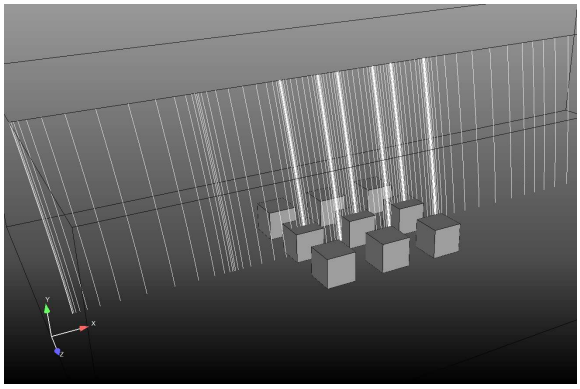

(c) *Rain trajectories, $d = 3.0$ [mm].*

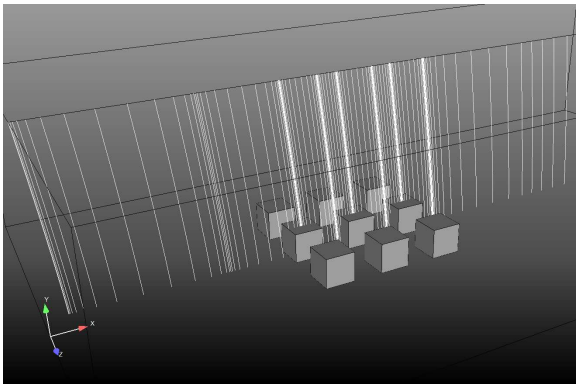

(d) *Rain trajectories, $d = 4.0$ [mm].*

Figure 3.7: *Rain phase trajectories along domain centerline.*

that the smaller diameter phases are much more heavily affected by the wind and thus should contribute more heavily to WDR than the larger diameter phases. However this is not necessarily the case due to the lower volume fraction of these smaller diameter phases. In Figures 3.8 and 3.9 we show the results for WDR using 8 phases.

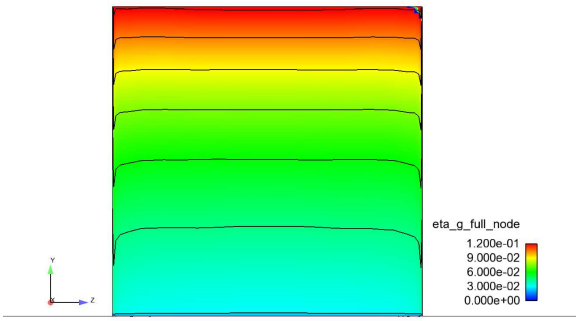

(a) η_{global} *values for cube A.*

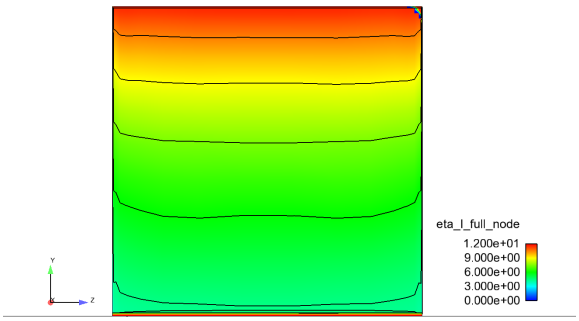

(b) η_{local} *values for cube A.*

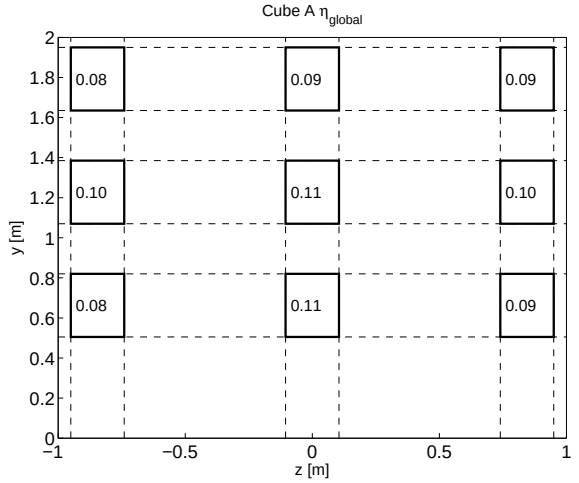

(c) *Simulation measurements at validation points on cube A.*

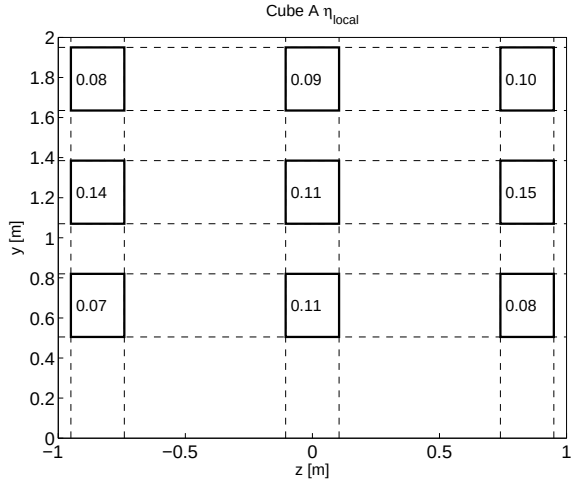

(d) *Simulation measurements at validation points on cube A.*

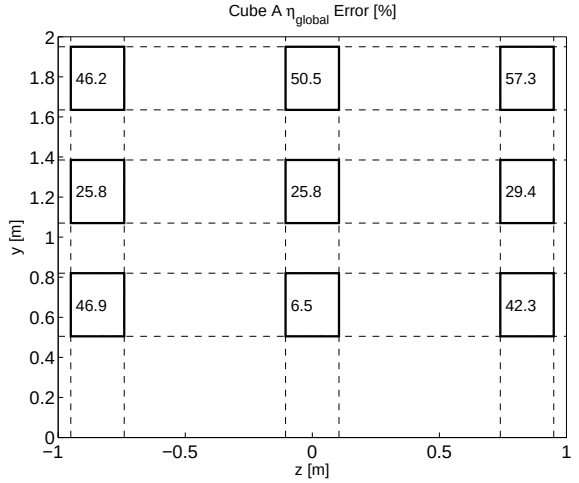

(e) *Error [%] between experiments and simulation:* η_{global}.

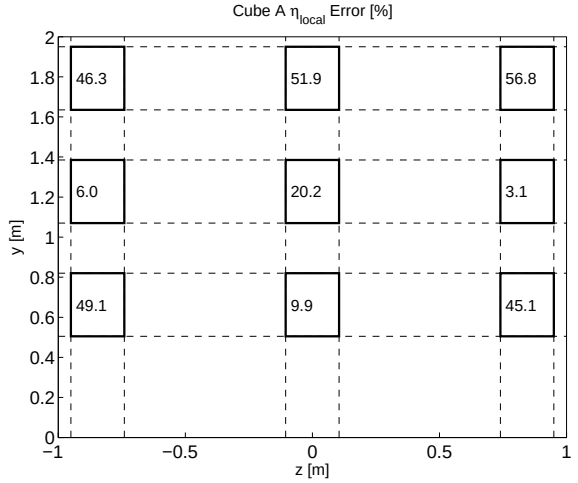

(f) *Error [%] between experiments and simulation:* η_{local}.

Figure 3.8: *Validation case results: Cube A, 8 phases.*

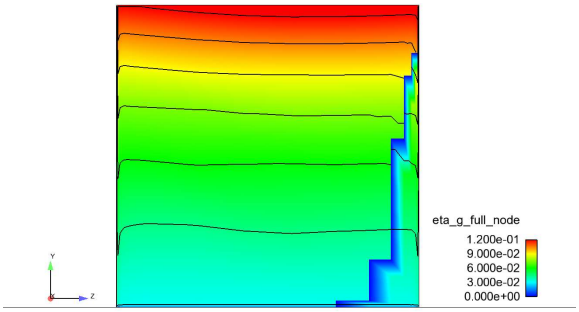

(a) η_{global} *values for cube B.*

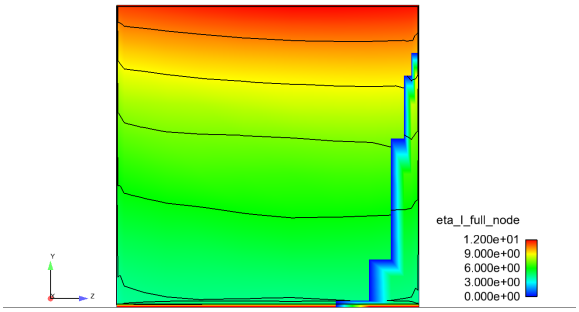

(b) η_{local} *values for cube B.*

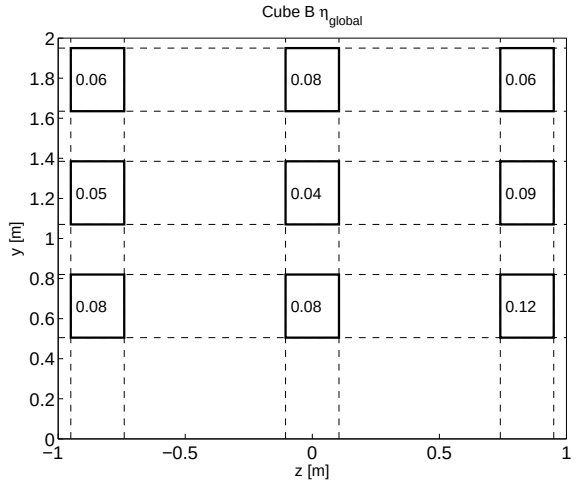

(c) *Simulation measurements at validation points on cube B.*

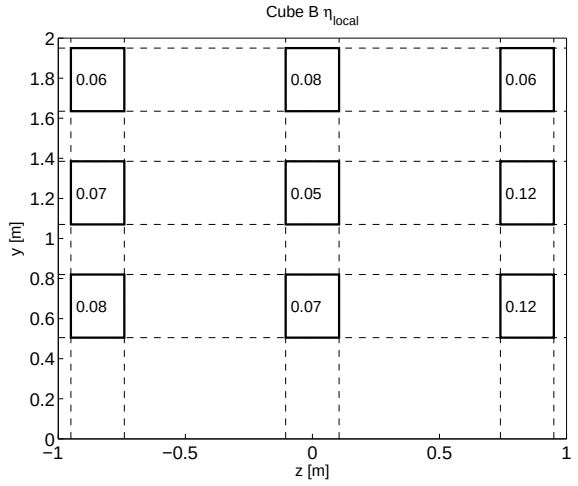

(d) *Simulation measurements at validation points on cube B.*

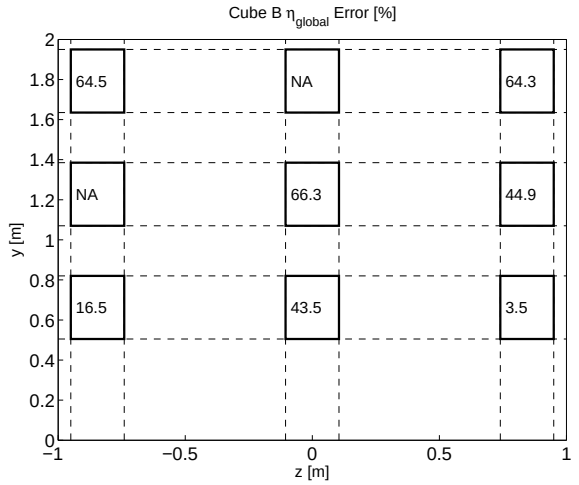

(e) *Error [%] between experiments and simulation:* η_{global}.

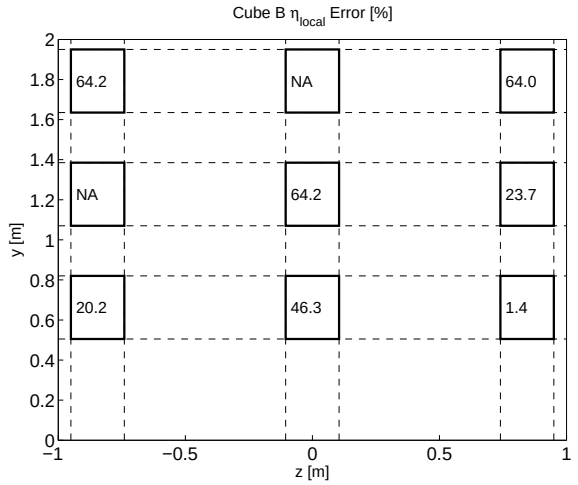

(f) *Error [%] between experiments and simulation:* η_{local}.

Figure 3.9: *Validation case results: Cube B, 8 phases.*

Unlike the 4 phase results we find that the global volumetric ratio calculation gives a higher error than that from the local ratio method. This is systemic over both cube A and B in places where there is error discrepancy. It is interesting to note that the error is lowest on all calculations in the center row of cube A and on the bottom row of cube B. This reflects the nature of the flow as well as the usage of the standard $k-\epsilon$ model with standard wall functions. The calculations are less accurate on the upper boundaries due to the model's over-prediction of turbulent kinetic energy on the top edge of the cubes and the flow separation is poorly predicted with this model, thus causing inaccuracies on the cubes situated behind the leading row.

The error results for cubes A and B using 4 and 8 phase methods are summarized in Table 3.5. If we

Location	Cube A				Cube B			
	4-phase		8-phase		4-phase		8-phase	
	η_{global}	η_{local}	η_{global}	η_{local}	η_{global}	η_{local}	η_{global}	η_{local}
Top L.	34.5	35.8	46.2	46.3	39.9	41.3	64.5	64.2
Top	53.4	56.2	50.5	51.9	NA	NA	NA	NA
Top R.	48.3	48.6	57.3	56.8	47.6	50.2	64.3	64.0
Mid. L.	13.0	19.1	25.8	6.0	NA	NA	NA	NA
Mid.	13.7	9.7	25.8	20.2	28.3	26.7	66.3	64.2
Mid. R.	14.7	16.6	29.4	3.1	39.1	19.0	44.9	23.7
Bot. L.	45.8	50.0	46.9	49.1	8.0	1.0	16.5	20.2
Bot.	41.8	46.2	6.5	9.9	32.4	37.3	43.5	46.3
Bot. R.	35.9	40.1	42.3	45.1	18.6	10.9	3.5	1.4

Table 3.5: Summary of errors [%] for all results of validation case.

compare the results of both calculations we can say that when using the global volumetric ratios we find that the error of using 4 phases is smaller than that of using 8 phases. This result is generally contradictory to what we would expect since we are making more assumptions on the raindrop sizes with the 4 phase model. The reason for the result can possibly be due to the increased stability we get when using a simulation with less phases. If we look at the results using the local volumetric ratio method for both phase models there is no clear superior model. In general we can state that again the model with less phases performs better in terms of error but this is not as consistent as in the global case. The inconsistency is likely to stem from the nature of the local ratio calculation, which is time averaged over an interval determined by the stability of the local velocity in the points where we measure.

4 Model 2: Skånegatan 1-3

The second simulation carried out focuses on the building located at Skånegatan 1-3, 411 40 Göteborg, Sweden; located at 57.7°42′24.4”N and 11°59′2.5”E and pictured in Figure **??**. This complex has representative height $H = 58$ meters.

4.1 Domain

The model is constructed in ICEM using architectural plans provided by the Building Technology Division, Civil and Environmental Engineering Department, Chalmers tekniska högskola. The domain boundaries are determined by standard practices and the blockage percentage is calculated to be around 1%. In Figures 4.1 and 4.2 we show the domain and a zoom on the building configuration, respectively.

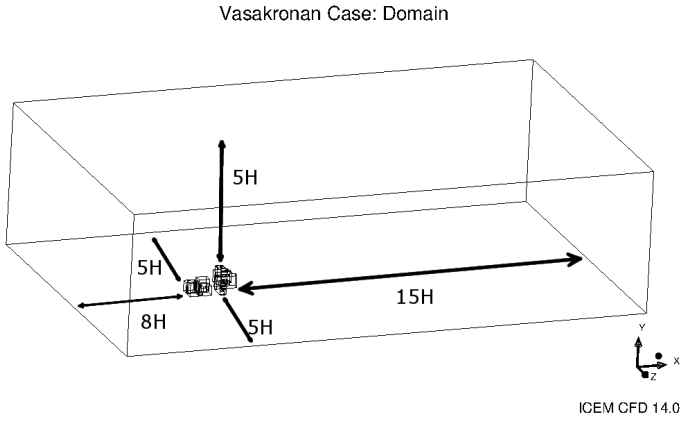

Figure 4.1: *Full domain, Skånegatan 1-3* .

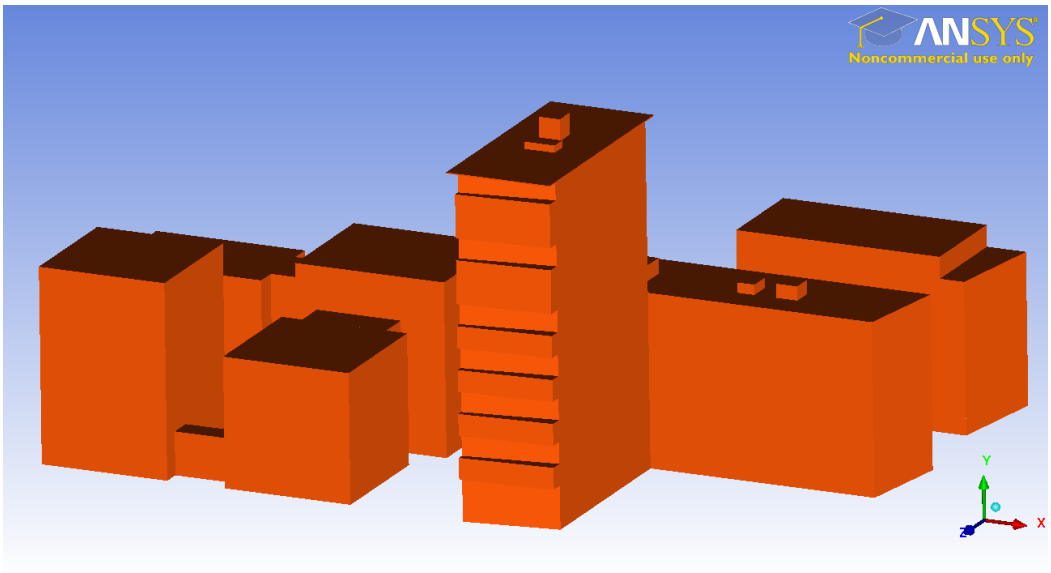

Figure 4.2: *Building configuration (zoom), Skånegatan 1-3.*

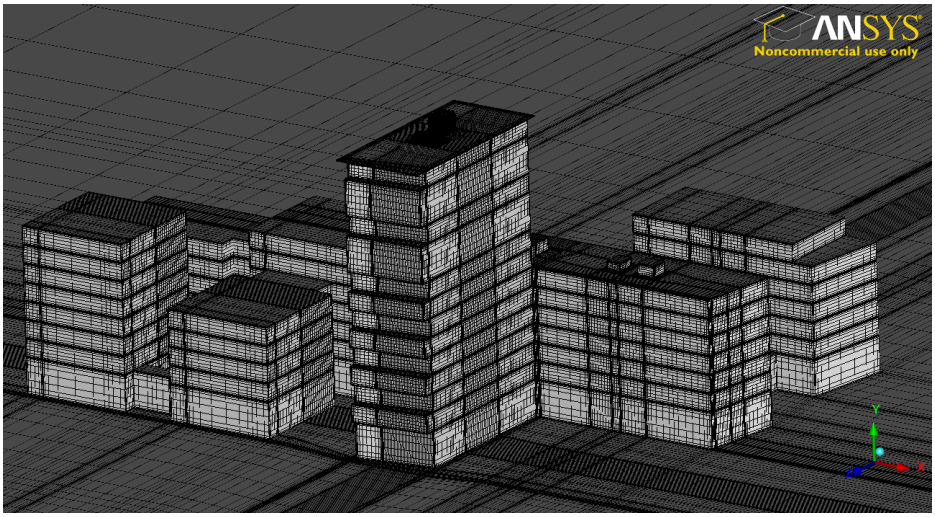

Figure 4.3: *Mesh zoom, Skånegatan 1-3.*

One compromise on the building itself is that the balconies on the side of the building must be projected slightly outwards from the facade to allow for better quality meshing. Additionally the roof is modeled as flat for simplicity in meshing whereas in reality the roof is slightly beveled. Note that the adjacent building complexes have been roughly modeled in order to provide accurate urban canyon effects in terms of WDR blockage and wind eddying. The model specifics are given in Table 4.1.

P [hPa]	$U(10)$ [m/s]	$U(30)$ [m/s]	Wind dir.	R_h [mm/hr]	T [K]
1010.5	7.5	15.4	163	3	283.25

Table 4.1: Meteorological data for Skånegatan 1-3.

We calculate the grid dimensions and element restrictions determined by the atmospheric conditions and turbulence model and present them in Table 4.2. The resulting mesh, pictured in Figure 4.3 consists of 14,341,622 hexahedral elements.

Dimension	Length [m]
$x(min)$	-368.8
$x(max)$	919.33
Δx	0.03
$y(min)$	0.0
$y(max)$	348.0
Δy	0.012
$z(min)$	-399.5
$z(max)$	383.7
Δz	0.012

Table 4.2: Domain and meshing information, Skånegatan 1-3.

4.2 Wind phase B.C.s

The building facade is assigned a no-slip wall condition with no roughness parameter, similarly to the cubes in the validation case. The ground condition is the same as the building facade with the addition of roughness. The roughness in this case has been increased somewhat to reflect the nature of the combination of grass, tram tracks and asphalt present in the vicinity of the building. The roughness height is 0.01 [m] and the roughness constant is kept at 0.5 to reflect Nikuradse's sand grain experiments. The inlet conditions are developed similarly to the validation case however the log-law formula is no longer sufficient to model the entire ABL present in this simulation, therefore we need to utilize the power law in addition to the log-law. The formulas for the velocity profile are (2.55) and (2.56). We also use equations (2.57) and (2.60)-(2.64) for the turbulent inlet profile values. Note that the turbulent intensity equation relies on the Coriolis force and latitude of interest and is only valid for temperate climates. The approximation is appropriate for Göteborg as the city lies in this region. The constants used in this simulation are

$$y_0 = 0.7, \tag{4.1}$$
$$\kappa = 0.42, \tag{4.2}$$
$$y_r = 30.0, \tag{4.3}$$
$$u_r = 15.4, \tag{4.4}$$
$$u^*_{ABL} = 1.7107 \text{ [m/s]}, \tag{4.5}$$
$$\Omega = 7.2722 \times 10^{-5} \text{ [rad/s]}, \tag{4.6}$$
$$\lambda = 57.7^\circ\text{N}. \tag{4.7}$$

The top of the domain is treated with a symmetry condition. Once the steady-state wind flow is solved this condition will be altered to account for the rainfall.

4.3 Rain phase B.C.s

The building facade maintains its no-slip wall condition as does the ground boundary condition. The inlet conditions remain unchanged from the wind calculation, no rain is introduced here. The outlet conditions are identical to the wind phase conditions, there is no modification for the inclusion of the rain phases. The top boundary is modified with the inclusion of the rain phases to accommodate the rainfall. We treat the top as an inlet with fixed streamwise velocities for all phases taken from the corresponding velocity profile generated for the wind inlet. In addition to streamwise velocity components the rain phases are assigned vertical velocities corresponding to their terminal velocities. Lastly the volumetric ratios of all phases must be assigned, they are given in Table 4.3.

Phase #	α_k	d [mm]	V_t [m/s]
1 (wind)	.9999998685	-	-
2	4.95×10^{-8}	1.2	4.64
3	5.25×10^{-8}	2	6.49
4	2.95×10^{-8}	4	8.83

Table 4.3: Volumetric ratios for Skånegatan 1-3 model.

4.4 Simulation settings

As with Model 1, the simulation is run in AVL FIRE in two stages. In stage 1 the wind profile is solved using the SIMPLE method under steady-state assumption. We use the second order AVL Smart Relaxed discretization scheme for momentum, central differencing scheme for pressure (continuity) and first order upwind for turbulence. The wind phase is considered converged when pressure, momentum and the turbulent quantities reach scaled residuals of 10^{-6}.

In stage 2 we run the simulation as unsteady with constant inflow conditions. The chosen timestep for this calculation is $\Delta t = 0.0025$ and is estimated using the assumption of a CFL number equal to 5. Ideally this

should be much closer to 1 however this restriction will result in exceedingly large computation times. The same reasoning is used during the mesh construction as standard techniques result in meshes in excess of 40 million elements. The restrictions were relaxed somewhat to generate the current mesh of 14 million elements. The SIMPLE/PISO solver is once again used instead of the SIMPLE solver and the residuals, mass flux, and streamwise velocity at chosen points is monitored to determine convergence.

4.5 Results

4.5.1 Wind phase solution

In Figure 4.4 we show the wind profile solution around the buildings of interest. Note that once again we have regions of recirculation between the buildings. Of particular note is the behavior of the wind in Figure 4.4e as it flow over the top of the lower buildings. The recirculation region here is heavily disrupted by the very narrow gap between the buildings. This should cause significant reduction of WDR on the Skånegatan 1-3 complex. We expect to have lower WDR on the section of the complex that is below the obstructing building and increased WDR on the section above it due to the flow acceleration over the top obstructing building.

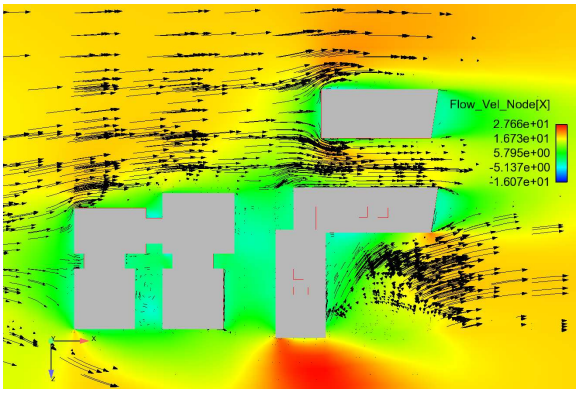

(a) *Streamwise wind velocity profile:* $y = 18$ *[m].*

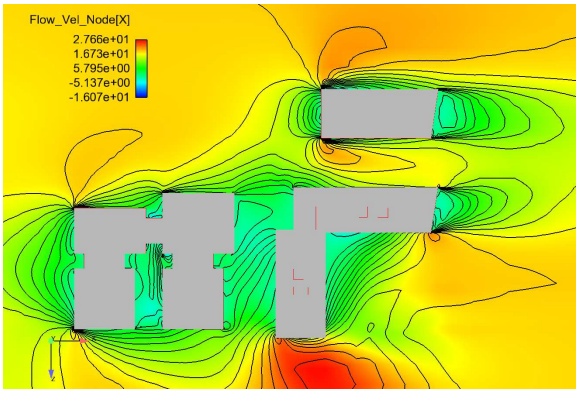

(b) *Streamwise wind velocity contour:* $y = 18$ *[m].*

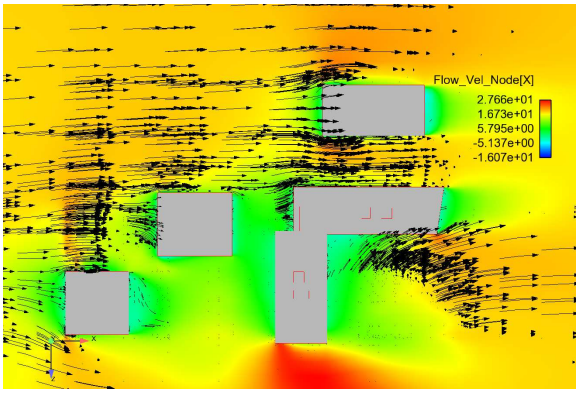

(c) *Streamwise wind velocity profile:* $y = 27$ *[m].*

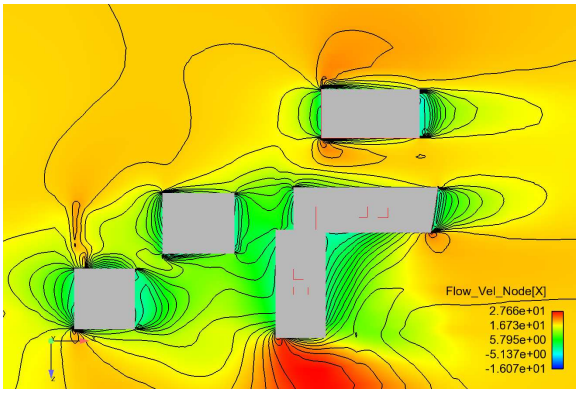

(d) *Streamwise wind velocity contour:* $y = 27$ *[m].*

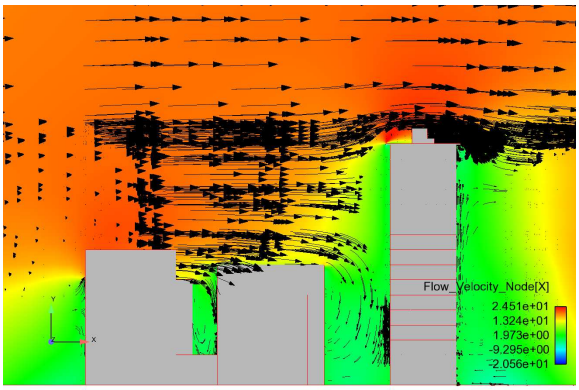

(e) *Streamwise wind velocity profile:* $z = 5.4$ *[m].*

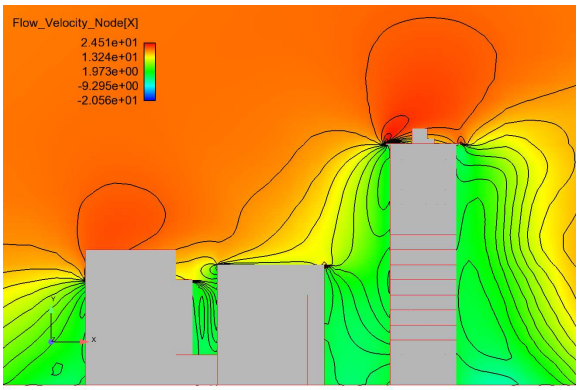

(f) *Streamwise wind velocity contour:* $y = 5.4$ *[m].*

Figure 4.4: *Domain cuts showing wind velocity profile [m/s].*

4.5.2 Rain phase solution

We run stage 2 of this case for 50 seconds and calculate the catch ratio using global volumetric ratio values. The reason for this is that we have established that this is more accurate than using the local values and since we have no data with which to compare, we do not require any such comparison. Note that at 50 seconds the simulation has not reached complete stability, this is due to the significant time requirements to reach a fully converged solution.

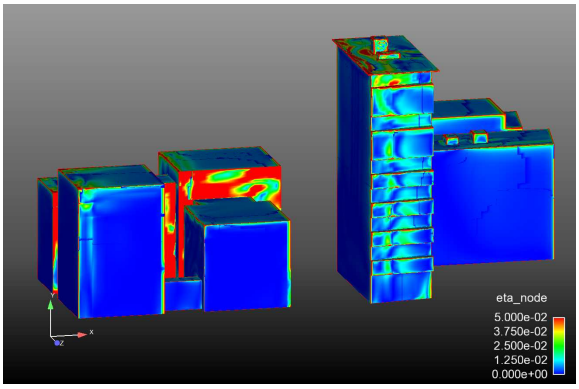

(a) η_{global} *distribution: view from east.*

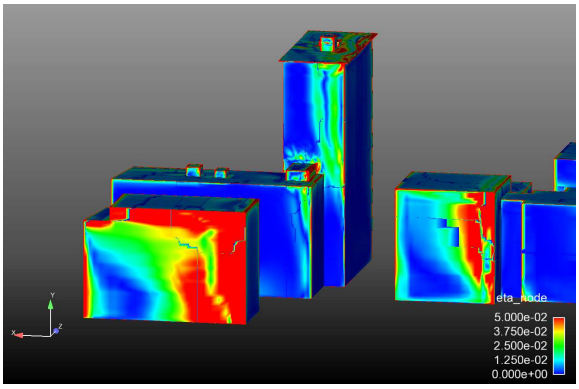

(b) η_{global} *distribution: view from west.*

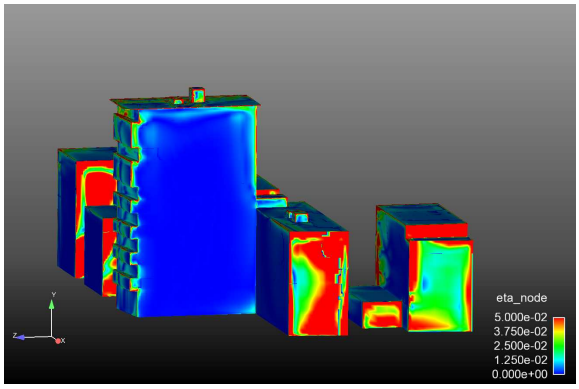

(c) η_{global} *distribution: view from north.*

Figure 4.5: *WDR distribution: Skånegatan 1-3.*

The results show that there is relatively low levels of WDR on the building sides themselves, this is most likely due to the overhang. Additionally we see that the balconies collect higher levels of WDR than the smooth sides. This is logical since the turbulence in these areas will increase and thus the areas experience higher lateral wind speeds, increasing WDR. The roof of the high-rise has very high levels of WDR when compared to the facades themselves. This is exactly the same as we see in the validation case, the only difference being the inconsistent nature of the distribution. We can see the cause is quite clearly the small perturbations on the roofs which disrupt the otherwise steady profile. It is interesting to see also the concentration of WDR on the windward side of the roof. This is most likely due to the simulation only having been run for 50 seconds, increased lengths of runtime should result in more uniform distribution of WDR on the rooftops, as well as the other sections of the facade. We can only get a general idea of the distribution pattern from these images and without any data for comparison these results should be taken only as a demonstration of the technique to a real-life case, not a precise solution of this particular model.

5 Conclusion and future work

In this paper we outline a method for calculating WDR using the Eulerian multiphase approach and solving the turbulent quantities using standard $k-\epsilon$ model for wind and rain phases. The approach consists of two stages wherein the wind profile is solved under steady-state conditions in stage 1 and is subsequently used as the initial solution for the introduction of the rain phases under unsteady conditions in stage 2. The simulations are run using AVL FIRE on two separate models, a validation case and highrise building complex in Göteborg, Sweden. The results for the validation case are compared to existing experimental data and the simulation is found to be within reasonable limits of accuracy. In addition to running the validation case with 4 phases we have run an 8 phase model as well. The findings of the results imply that there is no dramatic increase in solution accuracy when using more rain phases, and indeed the accuracy decreases slightly in the case of global volumetric ratios being used.

The major result of this paper is that the previous methodology can be extended to fully solving the rain phase turbulent equations and maintain result accuracy. This is quite important for future work on such modeling techniques however the result comes with several important considerations that need to be studied. The other important finding is that it may not be necessary to run these simulations with large numbers of rain phases, reducing the computational time and resources. The theoretical increase in accuracy from using more rain phases may be offset by numerical instability and increasing assumptions on the raindrop phase characteristics. In the following section we briefly discuss the challenges and assumptions affecting the simulation results.

5.1 Difficulties encountered in modeling WDR

We briefly discuss the variety of difficulties inherent with calculating WDR accurately. The methods described in section 2 are the current methods used to model WDR, however there are may sources of error within their construction. Additionally we must also consider software limitations, including settings such as boundary conditions and turbulence models as well as computational resources.

5.1.1 Methodological limitations

In this model we are using the standard $k-\epsilon$ model, which is known to be problematic for this type of simulation. With this in mind we can say that the accuracy of both the 4 phase and 8 phase validation case results are within acceptable boundaries, particularly when we consider previous work. For the previous work the errors were reported to be between 5% and 30%, averaged over an entire rain event whereas our results have errors from 1% to 66%. While the error spectrum is much larger than that of previous results it is fair to say the inclusion in this model of the full turbulent closure represents a step closer to a fully accurate method for calculating WDR.

For future research it is highly recommended to utilize an alternative turbulence model which performs better for these types of problems. The main issue with this will be the stability of the simulation in terms of turbulent quantities. Keep in mind that all of the inlet equations are valid only for $k-\epsilon$ models and must be altered to accurately reflect other turbulent model requirements. Additionally this author has experienced significant stability problems when attempting to run alternative turbulence models, though it is difficult to determine the reason for the instability. The possible reasons can include the boundary conditions, multiphase initialization and phase volumetric ratios, wall function choice and steady/unsteady conditions; to name a few. It is an important topic of further research to determine how drastically several of these parameters affect the stability of such simulations and exactly which assumptions can be made without altering the integrity of the simulation.

The other major methodological limitations present in this simulation are the definition of raindrop categories and their respective terminal velocities. There exist alternative methods to calculate the distribution and corresponding terminal velocities of raindrops present during rain events, however it is very difficult to asses the impact of such assumptions on WDR calculation.

5.1.2 Software and hardware limitations

One of the limitations of the approach outlined in this paper is computation time and resources, which is quite high with the inclusion of more phases, though our results show that this may not necessarily increase simulation accuracy. It takes substantial time and resources to run simulations with full multiphase, on the order of days for around 100 CPUs. This must be taken into account when comparing the method in this paper to previous works, though computation time is not reported in those papers.

Another technical limitation present in this approach is the software choice. In AVL FIRE it is impossible to assign phase-specific boundary conditions and additionally there is very little flexibility allowed even with with available boundary conditions. In this case the author must use wall conditions for all phases when modeling the building facades and ground. This is fine for the wind phase but as previously discussed this condition causes a large increase in the rain phase volumetric ratios on the facades. This makes it very hard to calculate WDR as one is forced to sample to the local volumetric ratio slightly away from the facade itself, creating a source of error. Ideally this can be solved by introducing phase-specific boundary conditions in AVL FIRE or by choosing an alternative software.

The final recommendation for future work is that more experiments be performed in order to accrue more data that can be used for validation purposes. This can include work done in wind tunnels or measurements taken under very specific conditions. Currently there is very little data that can be used for validation and even the existing data does not lend itself particularly well for validation of instantaneous simulations.

References

[1] M. Abuku et al. On the validity of numerical wind-driven rain simulation on a rectangular low-rise building under various oblique winds. *Building and Environment* **44** (2009), 621–632. DOI: 10.1016/j.buildenv.2008.05.003.

[2] A. C. Best. Size distribution of raindrops. *Quarterly J. Royal Meteorol. Soc.* 76 (1950), 16–36.

[3] B. Blocken and J. Carmeliet. Guidelines for the required time resolution of meteorological input data for wind-driven rain calculations on buildings. *Journal of Wind Engineering and Industrial Aerodynamics* **96**.5 (May 2008), 621–639. DOI: 10.1016/j.jweia.2008.02.008.

[4] B. Blocken, D. Derome, and J. Carmeliet. Rainwater runoff from building facades: A review. *Building and Environment* **60** (Feb. 2013), 339–361. DOI: 10.1016/j.buildenv.2012.10.008.

[5] B. Blocken and J. Carmeliet. A review of wind-driven rain research in building science. *Journal of Wind Engineering and Industrial Aerodynamics* **92**.13 (Nov. 2004), 1079–1130. DOI: 10.1016/j.jweia.2004.06.003.

[6] B. Blocken and J. Carmeliet. Spatial and temporal distribution of driving rain on a low-rise building. *Wind and Structures, An International Journal* **5**.5 (2002), 441–462.

[7] B. Blocken and J. Carmeliet. The influence of the wind-blocking effect by a building on its wind-driven rain exposure. *Journal of Wind Engineering and Industrial Aerodynamics* **94**.2 (Feb. 2006), 101–127. DOI: 10.1016/j.jweia.2005.11.001.

[8] B. Blocken and J. Carmeliet. Validation of CFD simulations of wind-driven rain on a low-rise building facade. *Building and Environment* **42**.7 (July 2007), 2530–2548. DOI: 10.1016/j.buildenv.2006.07.032.

[9] B. Blocken, T. Stathopoulos, and J. Carmeliet. CFD simulation of the atmospheric boundary layer: wall function problems. *Atmospheric Environment* **41**.2 (Jan. 2007), 238–252. DOI: 10.1016/j.atmosenv.2006.08.019.

[10] B. Blocken et al. The mutual influence of two buildings on their wind-driven rain exposure and comments on the obstruction factor. *Journal of Wind Engineering and Industrial Aerodynamics* **97**.5-6 (Aug. 2009), 180–196. DOI: 10.1016/j.jweia.2009.06.003.

[11] E. Choi. Determination of wind-driven-rain intensity on building faces. *Journal of Wind Engineering and Industrial Aerodynamics* **51** (1994), 55–69. DOI: 10.1016/0167-6105(94)90077-9.

[12] R. Gunn and G. D. Kinzer. *The Terminal Velocity of Fall for Water Droplets in Stagnant Air*. 1949. DOI: 10.1175/1520-0469(1949)006<0243:TTVOFF>2.0.CO;2.

[13] S. Huang and Q. Li. Numerical simulations of wind-driven rain on building envelopes based on Eulerian multiphase model. *Journal of Wind Engineering and Industrial Aerodynamics* **98**.12 (Dec. 2010), 843–857. DOI: 10.1016/j.jweia.2010.08.003.

[14] A. Kubilay et al. CFD simulation and validation of wind-driven rain on a building facade with an Eulerian multiphase model. *Building and Environment* **61** (Mar. 2013), 69–81. DOI: 10.1016/j.buildenv.2012.12.005.

[15] A. Kubilay et al. High-resolution field measurements of wind-driven rain on an array of low-rise cubic buildings. *Building and Environment* **78** (Aug. 2014), 1–13. DOI: 10.1016/j.buildenv.2014.04.004.

[16] A. Kubilay et al. Numerical modeling of turbulent dispersion for wind-driven rain on building facades. *Environmental Fluid Mechanics* **15**.1 (June 2014), 109–133. DOI: 10.1007/s10652-014-9363-2.

[17] A. Kubilay et al. Numerical simulations of wind-driven rain on an array of low-rise cubic buildings and validation by field measurements. *Building and Environment* **81** (Nov. 2014), 283–295. DOI: 10.1016/j.buildenv.2014.07.008.

[18] B. Launder and D. Spalding. The numerical computation of turbulent flows. *Computer Methods in Applied Mechanics and Engineering* **3**.2 (Mar. 1974), 269–289. DOI: 10.1016/0045-7825(74)90029-2.

[19] S. S. Mohaddes Foroushani, H. Ge, and D. Naylor. Effects of roof overhangs on wind-driven rain wetting of a low-rise cubic building: A numerical study. *Journal of Wind Engineering and Industrial Aerodynamics* **125** (Feb. 2014), 38–51. DOI: 10.1016/j.jweia.2013.10.007.

[20] J. Nikuradse. Gesetzmäßigkeiten der turbulenten Strömung in glatten Rohren (Nachtrag). *Forschung auf dem Gebiete des Ingenieurwesens* **4**.1 (Feb. 1933), 44–44. DOI: 10.1007/BF02716946.

[21] P. Richards and R. Hoxey. Appropriate boundary conditions for computational wind engineering models using the k-epsilon turbulence model. *Journal of Wind Engineering and Industrial Aerodynamics* **46-47** (Aug. 1993), 145–153. DOI: 10.1016/0167-6105(93)90124-7.

[22] Y. Tominaga et al. AIJ guidelines for practical applications of CFD to pedestrian wind environment around buildings. *Journal of Wind Engineering and Industrial Aerodynamics* **96**.10-11 (Oct. 2008), 1749–1761. DOI: 10.1016/j.jweia.2008.02.058.

[23] J. Wieringa. Representative roughness parameters for homogeneous terrain. *Boundary Layer Meteorology* **63**.4 (Mar. 1993), 323–363. DOI: 10.1007/BF00705357.

[24] Q.-s. Yang and J. Zhang. Simulation of Horizontally Homogeneous Atmosphere Boundary Layer Based on K-E Variant Models Combined With Modified Wall Functions. *The Seventh Asia-Pacific Conference on Wind Engineering* 2004 (2009), 1–8.

[25] Y. Yang et al. New inflow boundary conditions for modelling the neutral equilibrium atmospheric boundary layer in computational wind engineering. *Journal of Wind Engineering and Industrial Aerodynamics* **97**.2 (Feb. 2009), 88–95. DOI: 10.1016/j.jweia.2008.12.001.